Internal Report
DESY D3 - 78
July 1994

Studies on the Neutron Field Behind Side Shielding of a Target Bombarded with High Energy Protons

H. Dinter and K. Tesch

"Die Verantwortung für den Inhalt dieses
Internen Berichtes liegt ausschließlich beim Verfasser"

Internal Report
DESY D3 - 78
July 1994

Studies on the Neutron Field Behind Side Shielding of a Target Bombarded with High Energy Protons

H. Dinterand K. Tesch
Deutsches Elektronen-Synchrotron DESY
D - 22603 Hamburg, F. R. Germany

Abstract

Calculations using the Monte Carlo code FLUKA92 were performed to determine energy spectra and angular distributions of neutrons behind shielding of different thicknesses. A simple cylindrical geometry was adopted for the shielding materials concrete and iron. Boundary crossing and tracklength estimators were compared as well as fluence and current distributions, both for evaporation and high energy neutrons. Dose equivalents were calculated and parameters for an analytical formula were fitted. This formula enables to estimate dose equivalents in an easy way and represents a simple tool for practical applications in radiation protection. The predictions of the formula are compared with experimental data and good agreement was found.

1. Introduction

The Monte Carlo program FLUKA in its present version is able to simulate hadronic cascades and to create and to transport neutrons down to very low energies. This feature is of particular interest for radiation protection purposes because it enables to determine neutron energy spectra behind shielding and as a consequence to calculate dose equivalents if an appropriate set of conversion coefficients is applied.

Usually the geometry of the shielding of a high energy accelerator is a complicated arrangement of materials and even if it is possible to model it by means of 'combinatorial geometry' it takes a lot of effort and computer time to result in reliable values of dose equivalents. Therefore it is desirable for routine work in radiation protection to have a sort of 'catalogue' of the characteristics of the neutron field behind shielding for a standardized geometry that approximates really existing geometries.

Following this idea we used a simple cylindrical arrangement of target, shielding and detectors. We calculated the angular distribution of neutrons escaping shielding of different thicknesses, determined energy spectra registered by several fictive detectors behind side shielding and compared the results of three 'flux-scoring' methods ('estimators').

The spectra obtained by FLUKA were analysed and neutrons resulting from different production processes such as evaporation and the high energy cascade were treated separately to study their attenuation in the shielding materials.

From energy spectra dose equivalent values were deduced. In this way parameters were obtained to fit in a simple formula for easy estimation of dose equivalents.

The predictions of this formula can be verified in comparing with experimental data measured with a neutron spectrometer in a test beam area at CERN.

2. Calculational Method

We used **FLUKA92** for the main calculations of the present report [Fa92]. They are based on the simple cylindrical **geometry** which is shown in Fig. 1 and which is defined as *'The Standard Geometry'*.

A **beam** of protons of 100 GeV with a gaussian profile (FWHM is 5 mm) hits a cylindrical **target** with its axis parallel to the beam direction, in the center of its front face. The target material is iron, the length amounts to 2 m and the diameter to 10 cm.

The distance between the beam axis and the **shielding** surface was chosen as 1 m throughout all calculations. The shielding thickness was varied from 80 cm to 200 cm in the case of concrete and from 40 cm to 150 cm for iron. The composition of the concrete is listed in Tab. 1.

The outer surface of the shielding is surrounded by four regions without material serving as **detectors**. They are arranged side by side and with a length of 1 m each in direction of the beam axis. Neutrons escaping the shielding and crossing a detector boundary are scored and processed to energy spectra.

The method of calculating 'flux-like' quantities is determined by **estimators** provided in FLUKA. The *Boundary Crossing Estimator* registrates all neutrons leaving the shielding and entering a detector and calculates *Current* or *Fluence*, as wanted. The *Tracklength Estimator* determines *Fluence* using the lengths of the particle tracks in a detector volume. In the following calculations detectors with cross sections of 1 m (in z-direction) times 20 cm (in radial direction) of the detector rings was chosen (Fig. 1). No attempt was made to study the influence of the detector volume on the fluence.

For remembrance:

Current is defined as the number of particles crossing a scoring area divided by the size of the area. and
Fluence is defined as the sum of all particles, each divided by the cosine of the angle between its flight direction and the normal vector of the crossing area, divided by the size of the area.

To save computer time **energy cuts** were applied. Within the target volume as well as in the inner main part of the shielding neutrons were followed down to 1.5 keV. In a layer of 20 cm of the outer part of the shielding neutrons were maintained until thermal energies are reached and transported in this energy group with a survival propability of 0.5.

The **dose equivalents** behind the shielding were gained from fluence or current spectra by multiplying the value of each energy group with an appropriate conversion coefficient. In this report we use the coefficients of ICRP21, giving maximum dose equivalents in a semiinfinite slab of tissue equivalent material for a unidirectional broad beam with normal incidence.

3. Results

3.1 Energy Spectra

All neutrons crossing a boundary of interest are scored and sorted in terms of the polar angle θ, with its axis ($\theta = 0°$) in beam direction, in angle bins of 20°.

The energy distributions of neutrons entering the side shield are displayed in Figs. 2 to 4 for the angle bins 20°to 40°, 60°to 80° and 120°to 140°. In Figs. 5 to 10 distributions of neutrons of the same angular bins are shown leaving 80 cm of concrete or 40 cm of iron. All these figures show two clearly separated peaks, one around 100 MeV belonging to high energy cascade processes like spallation and another one in the 1 MeV-region caused by evaporation neutrons. The center of the evaporation peak depends in its energy on the shielding material. For concrete it lies around 2 MeV with a relatively sharp decrease down to 100 keV. Its intensity is roughly 1/4 of the high energy contribution. (see more details in section 3.3).

Behind iron the spectrum is completely different. The high energy neutrons behind 40 cm of iron amount approximately to the same number as that behind 80 cm of concrete. But in contrary to concrete the evaporation neutrons are 8 times more than the high energy neutrons. Its maximum lies around 400 keV and a soft decrease down to 1 keV is found. The small peak between 20 and 40 keV is significant and results from a minimum in the total absorption cross section.

All figures show that a separation of the two neutron components originating from the two different interaction mechanisms can clearly be made by integrating the spectra in two energy intervalls, one between 10^4 eV (10^3 eV for iron) and 10^7 eV including evaporation neutrons and a second one between 10^7 eV and the end of the spectra for high energy neutrons.

The energies of the neutrons cover a range of 12 orders of magnitude and therefore it is convenient to use a logarithmic energy scale for the display of the spectra. The energy groups in which the neutrons are sorted are logarithmically equidistant. Fluences (or currents) of each bin are divided by the logarithmic bin width ($\log(E_2/E_1)$ = 'unit lethargy') and plotted in a linear scale. In this way the area under the curve between two energies is proportional to the fluence in that intervall independent of the energy.

A consequence of this method is that the fluence at high energies is compressed in a way that may be misleading. As an example, the high energy cascade neutrons in all spectra appear as "peaks" with maxima around 100 MeV. Spectra plotted in a linear energy scale do not show such a peak between 10 and 500 MeV, but a flat distribution decreasing with energy.

In the Figures 11 and 12 the spectrum behind 80 cm of concrete is plotted in linear and logarithmic energy scales for comparison, no peak around 100 MeV exists in the linear plot. Such a distribution is expected if the cross sections of inelastic interactions of the nuclear cascade are studied.

In contrary to the high energy neutrons, the evaporation neutrons show a real peak between 1 and 5 MeV.

3.2 Angular Distributions

To obtain angular distributions, for each angle bin the number of particles are summed over all energy bins within the integrating intervall and divided by the solid angle of the bin. The results are shown in Figs. 13 to 16.

The evaporation neutrons for both materials are emitted symmetrically to 90°as expected for a source of isotropcally radiating nuclei close to the surface and homogenously distributed. The symmetry is independent of the shielding thickness (even at "thickness zero").

High energy neutrons show a different angular characteristic. Particles entering the shielding are peaked in foreward direction with a maximum between 20° and 40°, as shown in Figs. 14 and 16. This maximum is shifted towards higher angles with increasing shielding thickness and approaches 90°at 160 cm of concrete or 120 cm of iron. The "remembrance" of the particles of their origin diminishes with the number of interactions while its isotropy augments.

3.3 Analysis of Neutron Spectra

Neutron spectra detected by means of the 4 detectors surrounding the shielding (see Fig. 1) were calculated for thicknesses of 80, 140 and 200 cm of concrete and for 40, 80 and 120 cm of iron.

For each detector spectra of current and fluence were determined, the latter with boundary crossing and tracklength estimator. Evaporation and high energy neutrons were treated separately and their contribution to the total fluence was studied in terms of the shielding thickness.

In the following, average values of fluences, currents and dose equivalents are considered resulting from the detectors 2 and 3, because of compatibility to former studies. These mean values do not represent the maximum values which are actually found in detector 3 and for higher thicknesses in detector 4, in agreement with section 3.2. In general, for radiation protection purposes we are interested in these maximum values. The effect of this discrepancy is discussed in section 3.4.

3.3.1 Variation of the Shielding Thickness

In the Figs. 18 to 23 fluence spectra of the boundary crossing estimator are presented behind concrete and iron, for 3 different thicknesses per material. For comparison the spectra of the neutrons leaving the lateral surface of the target are added in Fig. 17, both escaping the first half of the target (z = 0 to 1 m) and the second half (z = 1 to 2 m). The numerical values of the spectra are added in the Appendix.

As a result a clear independence of the spectra structures was found in the range of thicknesses under study, for concrete and iron as well. Numerical evaluations for each material show that the contributions of high energy neutrons to the total fluence (Φ_{hig}/Φ_{tot}) and that of the evaporation neutrons (Φ_{eva}/Φ_{tot}) differ less than 10% for all thicknesses. Both estimators give the same result. In Tab. 2 these ratios averaged over the thicknesses are listed.

3.3.2 Comparisons of the Estimators

From Tab. 2 we find that boundary crossing and tracklength estimators give very similar fluence spectra. Between current- and fluence spectra differences are found, as expected.

Both neutron components have different angular distributions as seen in section 3.2 and as a consequence current and fluence values have to be different. For an unidirectional beam and normal incidence both quantities are equal, but the more isotropy prevails, the more fluence and current diverge, until the fluence is a factor of 2 higher than the current (because the mean value of the cosine equals 1/2).

In Tab. 3 the ratios of current to fluence are listed for evaporation neutrons, high energy neutrons and the total neutron spectrum. For both shielding materials the ratios are close to 1/2 for the isotropically emitted evaporation neutrons, whereas for the high energy neutrons, being more unidirectional, a ratio of approximately 3/4 was found.

The column 4 of Tab. 3 shows the ratios of both fluence estimators, tracklength and boundary crossing. The ratios are constant throughout all calculations. Ratios close to unity are expected. The discrepancies result from the unfavourable choice of the detector volume.

3.4 Estimation of Dose Equivalents

The fluence and current values are the basis on which dose equivalents were calculated with the aim to get fitting parameters for a simple analytical expression that enables to estimate dose equivalents for routine purposes. As a fitting formula for the dose equivalent per beam particle H, the following ansatz was used:

$$H = H_0 \cdot (\frac{E_p}{GeV})^{0.8} \cdot f_T \cdot \frac{1}{r^2} \cdot e^{-\frac{d}{\lambda}},$$

where E_p is the energy of the proton beam, r is the radial distance between the beam axis and the location of interest, and d is the radial thickness of the shielding material, both in accordance with Fig. 1.

The magnitude f_T takes into account the dependance of the dose equivalent on the target diameter studied in another report [Di94]. For a target diameter of 10 cm f_T is defined as unity while for smaller diameters it diminishes according to Fig. 24.

This formula seems to describe the shielding of a pointlike source but it has to be emphasized that it represents only a fitting formula for the results of the calculations. The complicated processes of the hadronic cascades developed in the target and in the shielding and the interactions of the secondary particles with the shielding matter cannot be described in such a simple way, even not approximately. The magnitude λ defined in this way does not represent a pure dose attenuation coefficient belonging to a certain energy or angle, it is rather a fitting constant reflecting the effective attenuation of the integral dose equivalent of the global situation.

All calculations were performed at a beam energy of 100 GeV. For other energies the $E^{0.8}$-dependence of the dose equivalent was taken as proved [Th88]; the reasons are given in [Te91].

3.4.1 Calculation of the Fitting Parameters

Using the calculated values of H and the fitting formula, the missing parameters H_0 and λ can be deduced. The values Hr^2 are plotted as a function of the shielding thickness in Fig. 25. For all entries of both materials a clear exponential decrease is found. Hence it follows that H_0 and λ are constant, at least in the thickness region studied here.

As mentioned in section 3.3 the dose equivalents are calculated as an average for the detectors 2 and 3 (see Fig. 1). The maximum values however are found in detector 3 and even detector 4 for higher thicknesses. Therefore the fitting procedure was performed for doses gained by the 3 estimators for detectors 2+3 and in addition for the maximum dose. The results are summarized in Tab. 4.

The effective attenuation coefficients λ are independent of the type of estimator used and depend only on the shielding material. From the intercept of the straight line of the semilogarithmic plot of Fig. 25 the constant H_0 may be derived. It depends on the estimator (as concluded from Tab. 3) and on the material.

The ratios of the constants H_0 should equal the respective ratios of Tab. 3 (line H_{tot}). The unimportant deviations result from rounding errors and fitting uncertainties.

The difference between the maximum values of the dose equivalents and those found for detectors 2+3 amounts to 15% , as a possible underestimation (but see section 4.).

The variation of λ is very small and due to calculational effects. The mean values of λ (125. g/cm^2 for concrete and 153. g/cm^2 for iron) may be compared with coefficients published in other reports or review articles [Te86] , [Th88] , [Fa90]. They are listed in Tab. 5.

For the parameters H_0 the values obtained by the fluence of the boundary crossing estimator are favourable. Their overestimation of the experimental data (see Tab. 6) compensates for an underestimation of the same amount because of using the mean values of the doses of the detectors 2+3 instead of the maximum dose.

Generally, the choice of H_0 depends on the type of dose equivalent to be determined. As mentioned above ICRP21 conversion coefficients were used which means dose equivalents that represent maximum values in a slab phantom. However, applying them to the Standard Geometry is an approximation which does not agree with the assumptions of ICRP21. Other concepts exist as e. g. the commonly used ambient dose equivalent H*(10) but it underestimates the dose equivalent for neutrons of very high energies. Additional calculations were performed using conversion coefficients of ICRP51 together with coefficients extended in energy [St86]. Maximum deviations of 20% from ICRP21 values were found.

A general answere of the question which type of dose equivalent is relevant to a person standing behind the side shielding of a high energy accelerator is difficult to find.

Fortunately, the difference of the dose equivalent values determined by different concepts is not very high. Our aim was to find a method to estimate dose equivalents within a factor of 2, and within this context a difference of dose equivalents of 20 or 30% is completely unimportant.

3.4.2 Comparison with Experimental Data

In the framework of an international collaboration at CERN neutron spectra were measured by means of a neutron spectrometer, behind side shielding of 80 cm of concrete and 40 cm of iron. The experimental details and the summarized results are reported in [Di93] .

These experimental values can be compared with the predictions of the formula using λ = 125. g/cm^2 for concrete and λ = 153. g/cm^2 for iron together with the H_0-values of

Tab. 4 for fluence and current (boundary crossing estimator). But since no variation of the shielding thicknesses was possible only one experimental point can be contributed to Fig. 25. The results are shown in Tab. 6 for comparison.

The experimental data fit well between calculated currents and fluences for all three locations of measurement. However, a decision which one of both calculational methods (current or fluence) is the more appropriate cannot be met from this comparison. But anyway, it is of no practical importance because the differences between currents and fluences are less than 30% .

4. Summary and Recommendations

The results of this study are applicable to neutron fields behind a homogeneous lateral shielding of concrete or iron for high energy proton accelerators. They may be summarized in the following way:

1. The neutron field consists mainly in evaporation neutrons and high energy neutrons. The composition of both components depends highly on the shielding material.

2. Evaporation neutrons are isotropically emitted and behind shielding they are distributed symmetrically to 90°. High energy neutrons have an angular maximum between 60° and 90° depending on the shielding thickness.

3. The neutron spectra are independent of the shielding thickness.

4. Currents are around 0.6 times the fluences, averaged over the total energy range.

5. A simple formula for estimation of the dose equivalents is discussed.

6. Effective attenuation coefficients for dose equivalents were fitted for this formula. The recommended values are:
   $\lambda = 125.$ g/cm^2 for concrete and
   $\lambda = 160.$ g/cm^2 for iron.

7. "Source terms" were fitted for the formula. The recommended values are:
   $H_0 = 9 \cdot 10^{-15}$ Sv $\cdot$ m^2 for concrete and
   $H_0 = 3 \cdot 10^{-14}$ Sv $\cdot$ m^2 for iron.

8. Comparisons with experimental data show good agreement.

References

[Di93] H. Dinter, B. Racky and K. Tesch:
Measurements of Spectra and Dose Equivalents of High Energy Neutrons Behind Shielding
Laborbericht DESY D3 - 83 (1993).

[Di94] H. Dinter and K. Tesch:
A Simple Estimation of the Dose Equivalent Behind Shielding of High Energy Proton Accelerators
Proceedings of the Specialists' Meeting on Shielding Aspects of Accelerators, Targets and Irradiation Facilities, Arlington, Texas, 28 - 29 April 1994 (in press).

[Fa90] A. Fassò, K. Goebel, M. Höfert, J. Ranft and G. Stevenson. Editor H. Schopper:
Shielding Against High Energy Radiation
Landold-Börnstein, Numerical Data and Functional Relationships in Science and Technology, New Series, Vol. 11 (1990).

[Fa92] A. Fassò, A. Ferrari, J. Ranft, P. R. Sala, G. R. Stevenson and J. M. Zazula:
"FLUKA92"
Proceedings of the Workshop on Simulating Accelerator Radiation Environment, Santa Fe, January 11 - 15, 1993.

[St86] G. R. Stevenson:
Dose Equivalent per Star in Hadron Cascade Calculations
CERN, Divisional Report TIS-RP/173 (1986).

[Te86] K. Tesch and H. Dinter:
Estimation of Radiation Fields at High Energy Proton Accelerators
Rad. Prot. Dosimetry 15 (1986) 89.

[Te91] K. Tesch and J. M. Zazula:
Shielding properties of iron at high energy proton accelerators studied by a Monte Carlo code
Nucl. Instr. and Methods A300 (1991) 179.

[Th88] R. H. Thomas and G. R. Stevenson:
Radiological Safty Aspects of the Operation of Proton Accelerators
Technical Reports Series No. 283, IAEA, Vienna 1988.

Element Symbol	At.weight g/mol	Percent by weight
O	16.00	53.
Si	28.09	34.
Ca	40.08	4.
Al	26.98	3.
Na	22.99	2.
Fe	55.85	2.
H	1.01	1.
C	12.01	1.
Mg	24.31	1.
K	39.10	1.
ρ = 2.42 g/cm^3		

Table 1: Composition of ordinary concrete used at DESY and for the calculations.

Material	Ratio	BDX-cur	BDX-flu	TRL-flu
Concrete	Φ_{hig}/Φ_{tot}	0.60	0.54	0.55
	Φ_{eva}/Φ_{tot}	0.28	0.32	0.32
	Φ_{hig}/Φ_{eva}	2.14	1.69	1.72
	H_{hig}/H_{tot}	0.76	0.71	0.72
	H_{eva}/H_{tot}	0.23	0.28	0.27
Iron	Φ_{hig}/Φ_{tot}	0.061	0.045	0.051
	Φ_{eva}/Φ_{tot}	0.79	0.80	0.79
	Φ_{hig}/Φ_{eva}	0.077	0.056	0.065
	H_{hig}/H_{tot}	0.22	0.17	0.19
	H_{eva}/H_{tot}	0.77	0.82	0.80

Table 2: Contributions of evaporation neutrons and high energy neutrons to the total fluence and current. The figures represent the mean values of the calculated ratios behind 3 shielding thicknesses. (BDX = boundary crossing estimator; TRL = tracklength estimator).

Material	Φ, H	Cur/Flu	TRL/BDX
Concrete	Φ_{tot}	0.67	0.87
	Φ_{hig}	0.74	0.89
	Φ_{eva}	0.58	0.85
	H_{tot}	0.70	0.88
Iron	Φ_{tot}	0.56	0.80
	Φ_{hig}	0.76	0.86
	Φ_{eva}	0.53	0.77
	H_{tot}	0.58	0.80

Table 3: Comparison of estimators (BDX = boundary crossing; TRL = tracklength). Cur/Flu means the ratios of current to fluence values of the boundary crossing estimator.

	Concrete		Iron	
	λ (g/cm^2)	H_0 (Sv· m^2)	λ (g/cm^2)	H_0 (Sv· m^2)
BDX-current	124.	$5.9 \cdot 10^{-15}$	151.	$2.3 \cdot 10^{-14}$
BDX-fluence	123.	$8.5 \cdot 10^{-15}$	156.	$3.4 \cdot 10^{-14}$
TRL-fluence	126.	$7.0 \cdot 10^{-15}$	152.	$3.1 \cdot 10^{-14}$
Max. fluence	128.	$1.0 \cdot 10^{-14}$		

Table 4: Fitting parameters λ and H_0 for the dose equivalents of detectors 2+3 and for 3 different estimators. The last line stands for the maximum dose values.

	Concrete	Iron
Reference	λ (g/cm^2)	λ (g/cm^2)
[Te86], [Te91]	107.	180.
[Th88]	117.	170.
[Fa90]	133.	164.
Present work	125.	153.

Table 5: Comparison of λ values of the present study and of formerly published data.

Shielding material	Thick-ness	Loc.	Calculations		Experiment
			Current	Fluence	
Concrete	80 cm	top	$2.0 \cdot 10^{-10}$	$2.9 \cdot 10^{-10}$	$2.3 \cdot 10^{-10}$
	80 cm	side	$2.4 \cdot 10^{-10}$	$3.5 \cdot 10^{-10}$	$3.5 \cdot 10^{-10}$
Iron	40 cm	top	$7.4 \cdot 10^{-10}$	$1.1 \cdot 10^{-9}$	$8.7 \cdot 10^{-10}$

Table 6: Comparison of measured and calculated dose equivalents in Sv per count of the beam monitoring ionization chamber (PIC). 1 PIC-count equals to $2.0 \cdot 10^4$ beam particles.

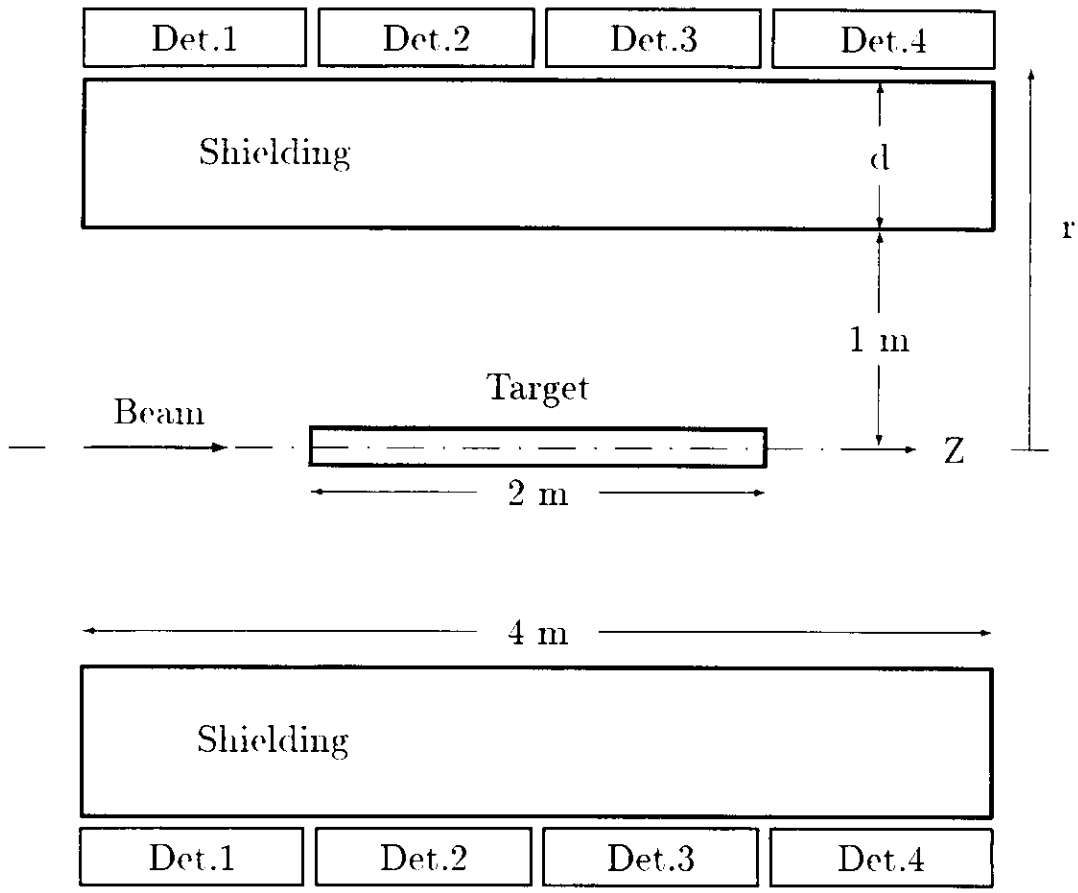

Figure 1: The Standard Geometry

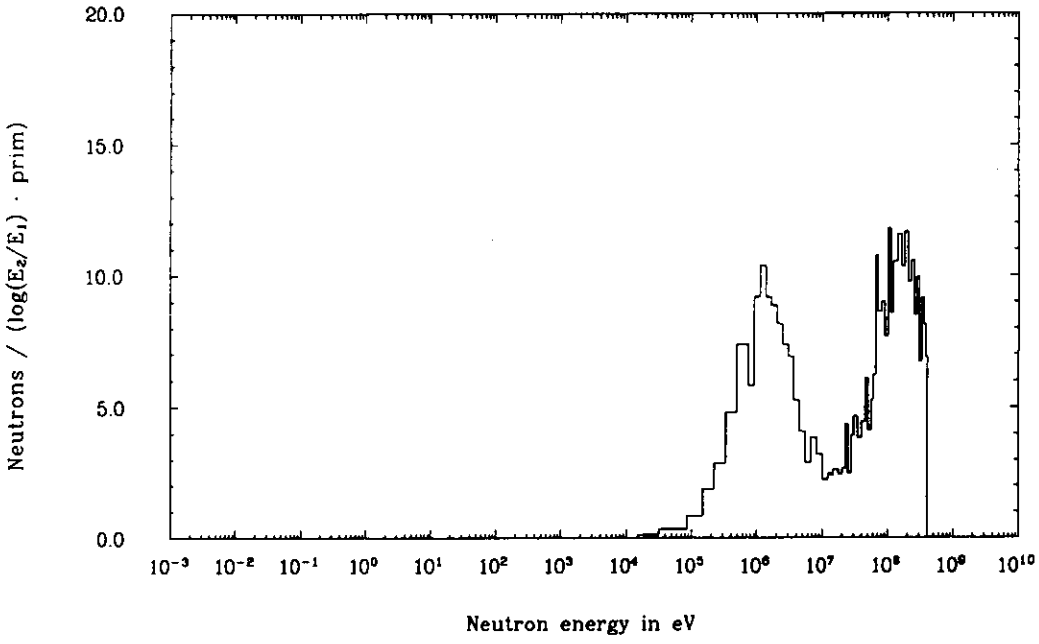

Figure 2: Energy distribution of neutrons entering the side shielding in a polar angle bin 20° to 40°.

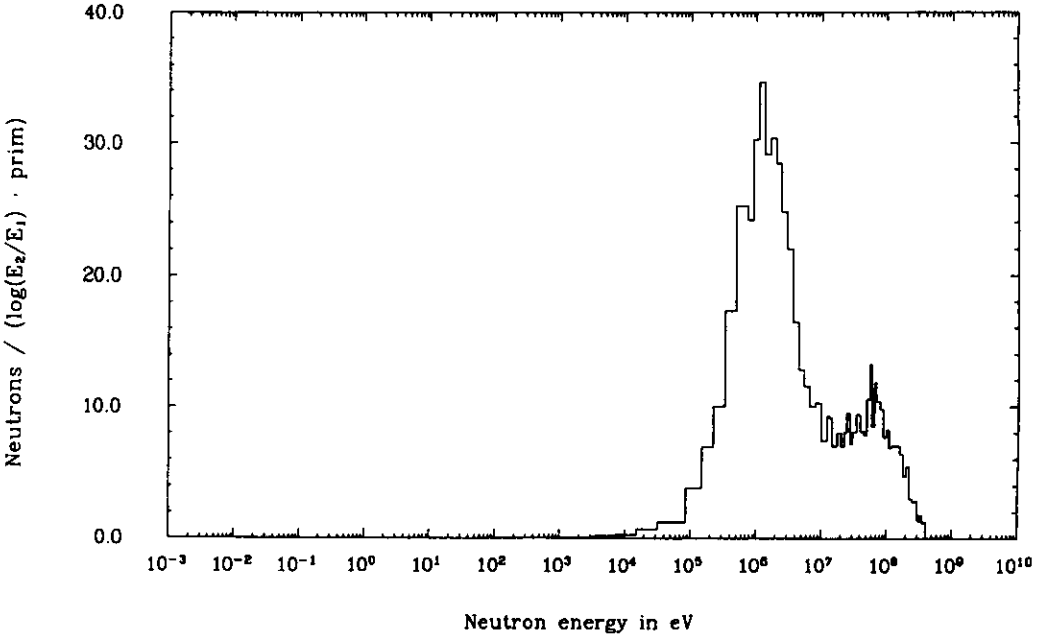

Figure 3: Energy distribution of neutrons entering the side shielding in a polar angle bin 60° to 80°.

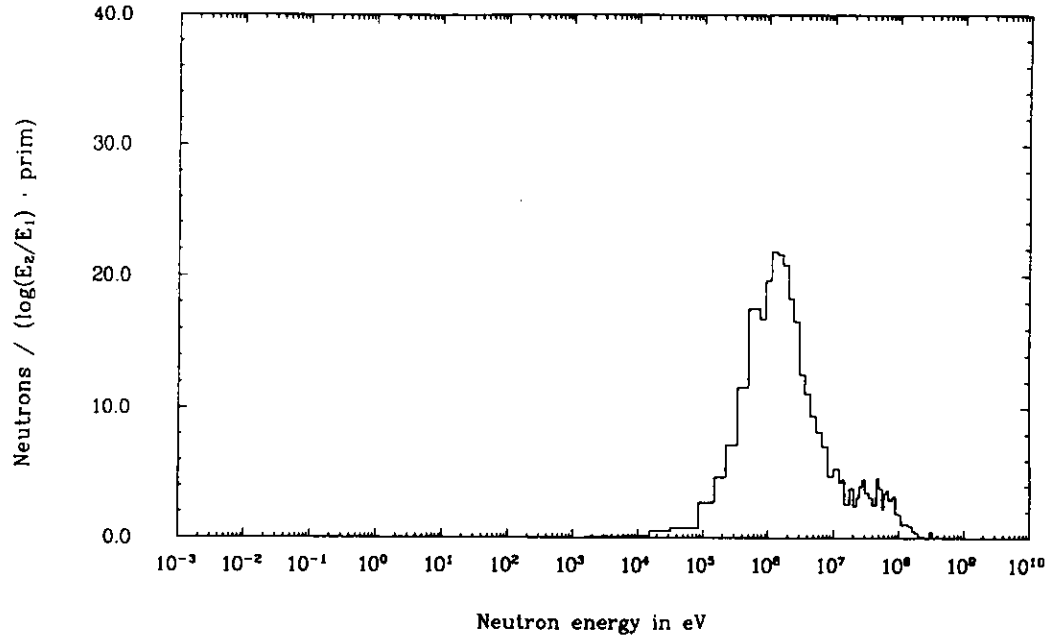

Figure 4: Energy distribution of neutrons entering the side shielding in a polar angle bin 120° to 140°.

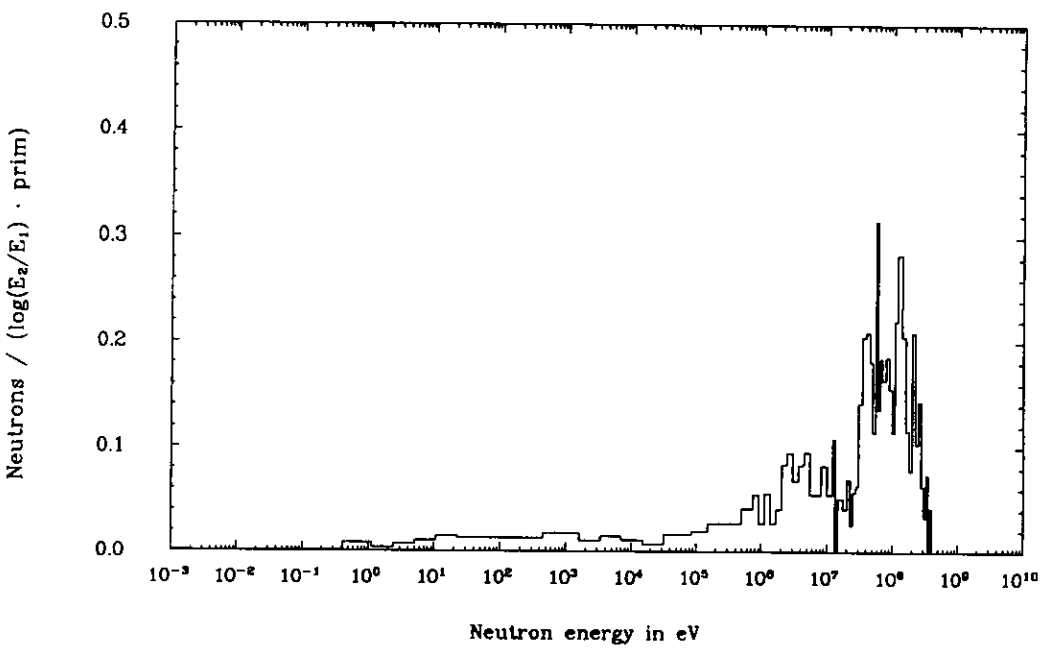

Figure 5: Energy distribution of neutrons behind 80 cm of concrete in a polar angle bin 20° to 40°.

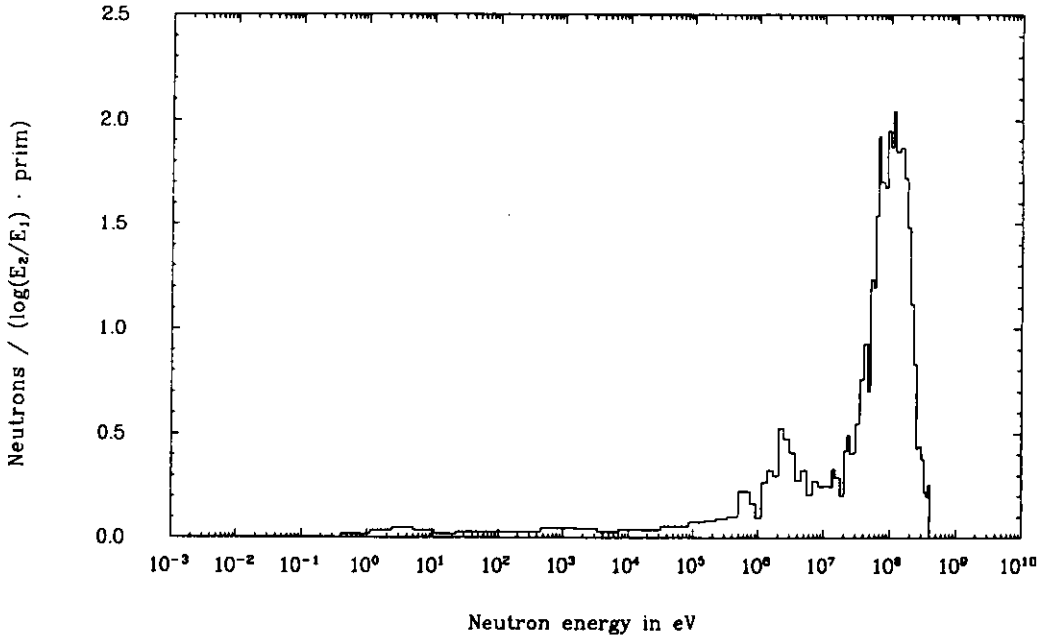

Figure 6: Energy distribution of neutrons behind 80 cm of concrete in a polar angle bin 60° to 80°.

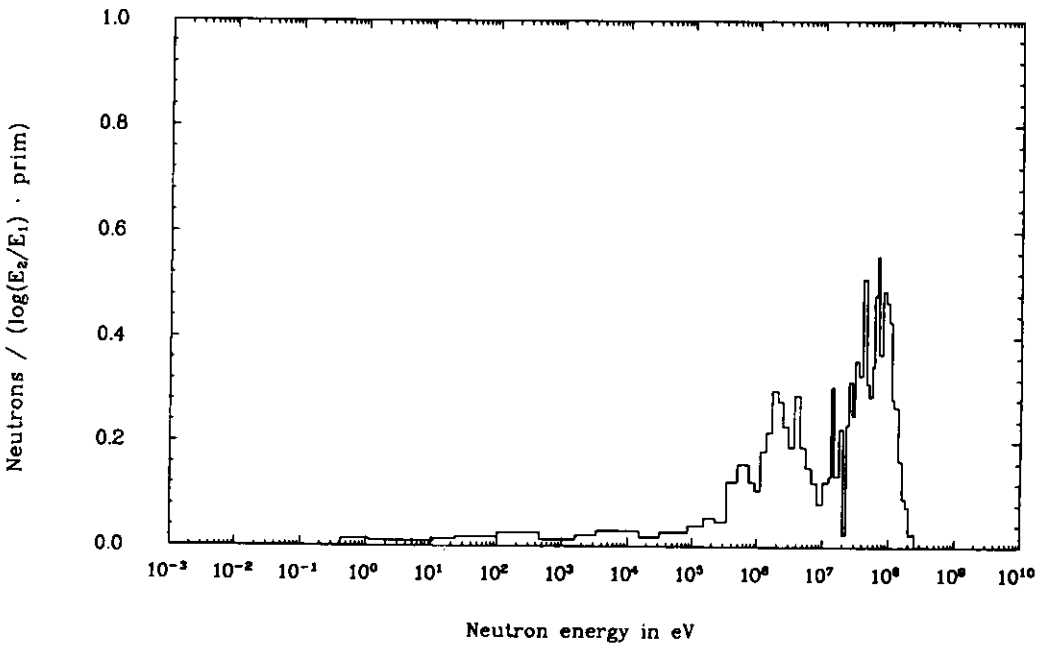

Figure 7: Energy distribution of neutrons behind 80 cm of concrete in a polar angle bin 120° to 140°.

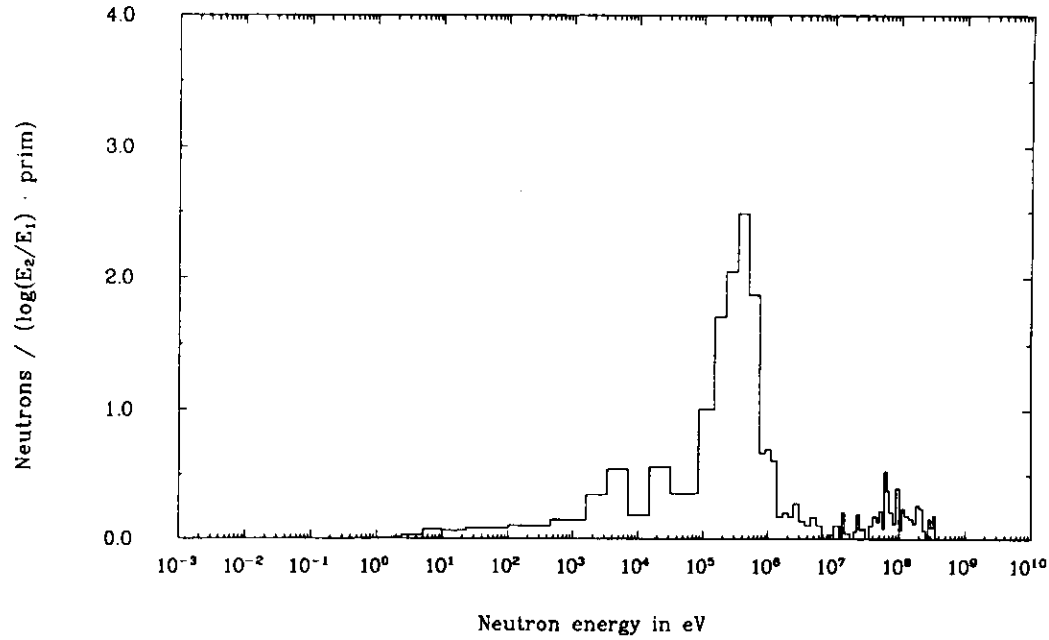

Figure 8: Energy distribution of neutrons behind 40 cm of iron in a polar angle bin 20° to 40°.

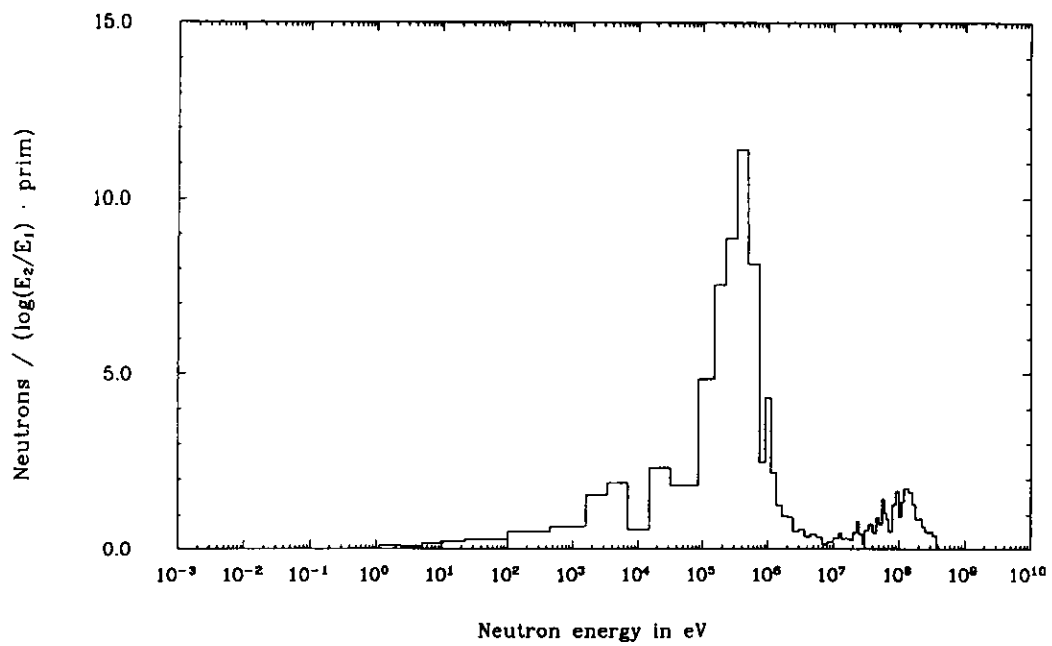

Figure 9: Energy distribution of neutrons behind 40 cm of iron in a polar angle bin 60° to 80°.

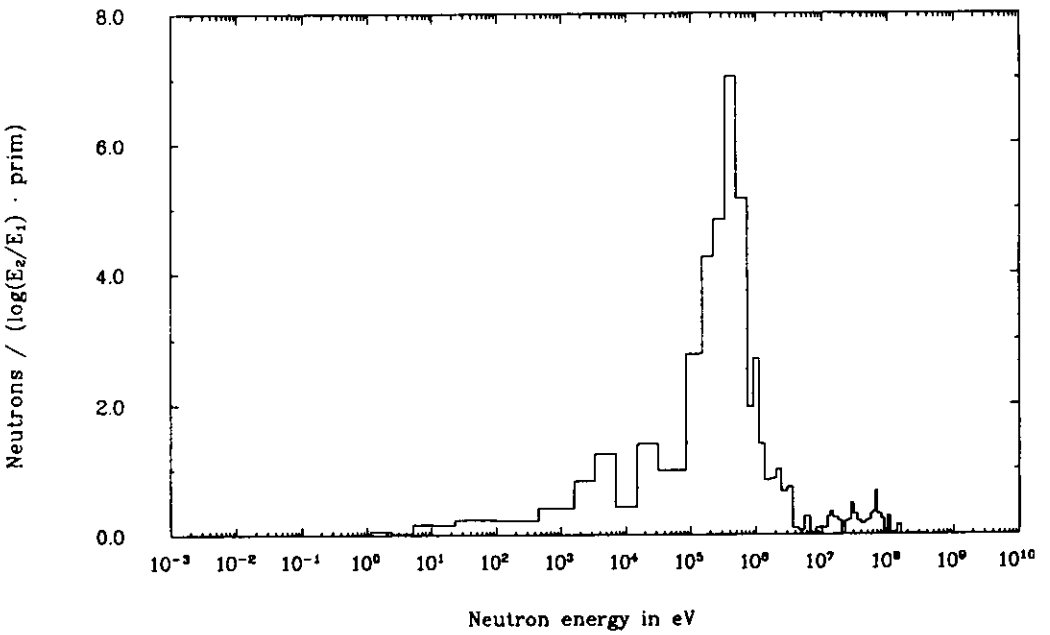

Figure 10: Energy distribution of neutrons behind 40 cm of iron in a polar angle bin 120° to 140°.

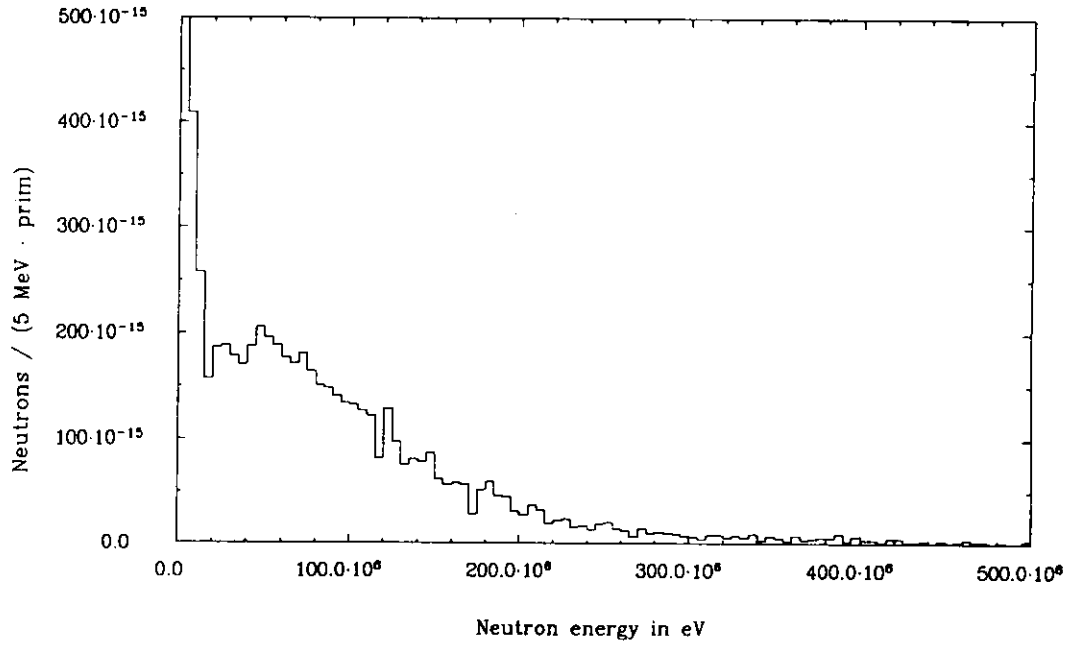

Figure 11: Energy distribution of neutrons behind 80 cm of concrete. Displayed in a linear energy scale.

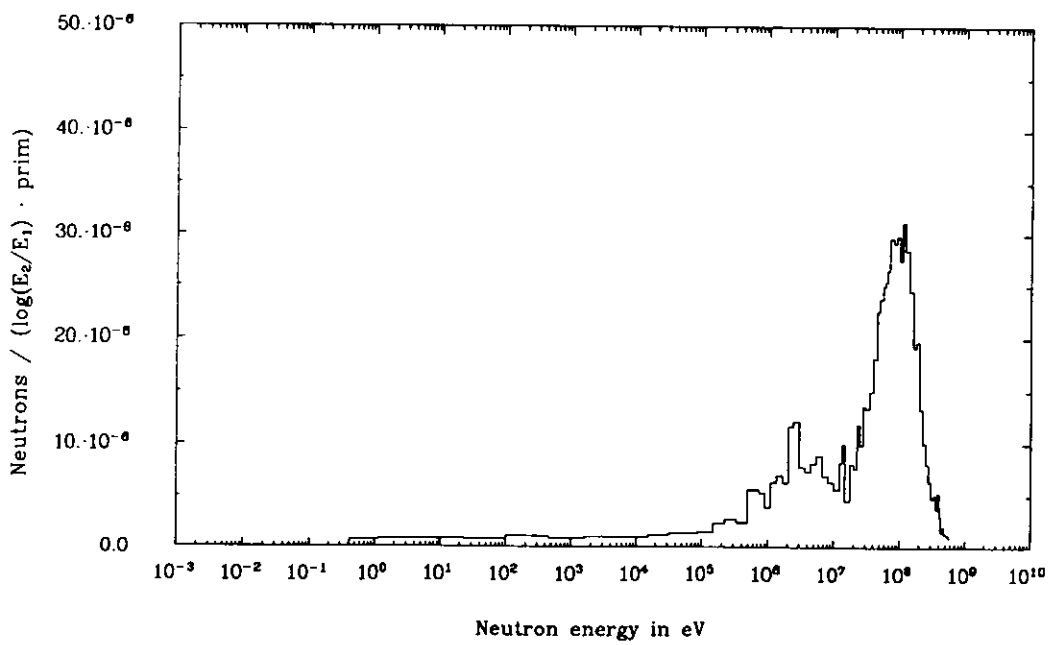

Figure 12: Energy distribution of neutrons behind 80 cm of concrete. The same spectrum as above but displayed in a logarithmic energy scale.

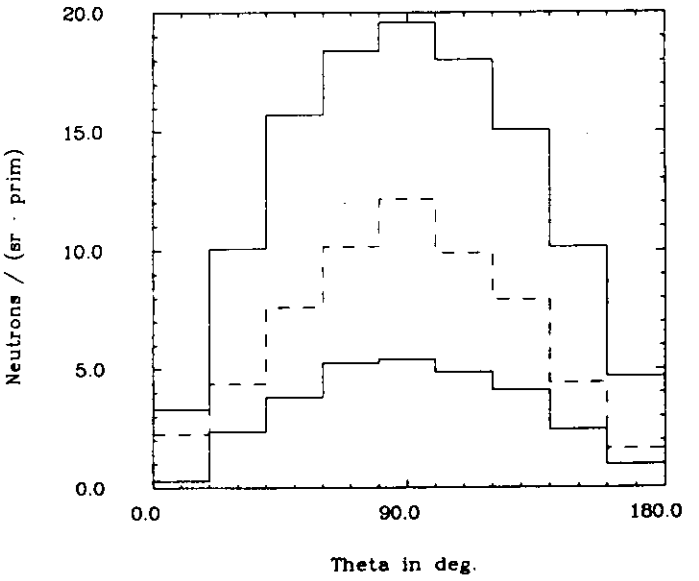

Figure 13: Angular distribution of evaporation neutrons (energy intervall 0.91 to 13.5 MeV). Top graph: neutrons escaping the target; Middle (scale div. by 40): neutrons leaving 80 cm concrete: Bottom (scale div. by 50): neutrons leaving 160 cm concrete.

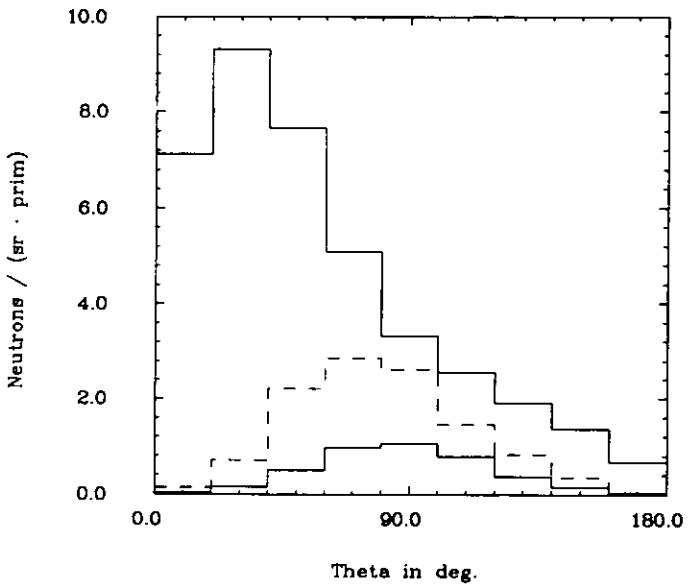

Figure 14: Angular distribution of high energy neutrons (energy intervall 14.9 to 400. MeV). Top graph: neutrons escaping the target; Middle (scale div. by 4): neutrons leaving 80 cm concrete; Bottom (scale div. by 10): neutrons leaving 160 cm concrete.

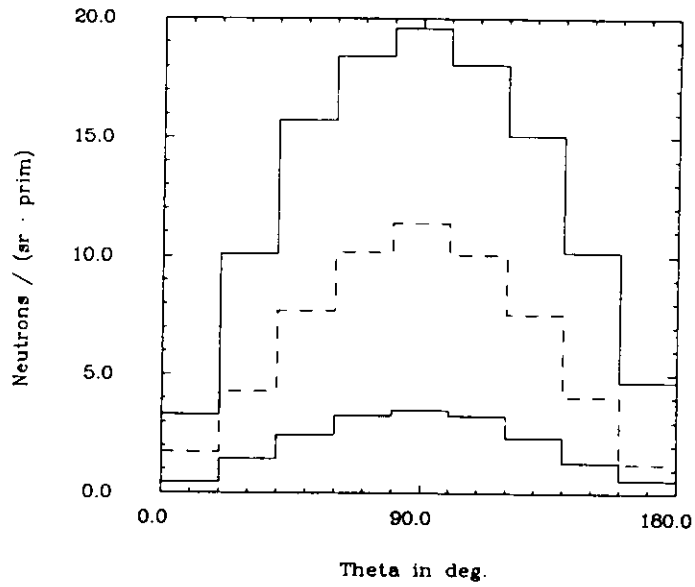

Figure 15: Angular distribution of evaporation neutrons (energy intervall 0.91 to 13.5 MeV). Top graph: neutrons escaping the target; Middle (scale div. by 2): neutrons leaving 40 cm iron; Bottom (scale div. by 6): neutrons leaving 80 cm iron;

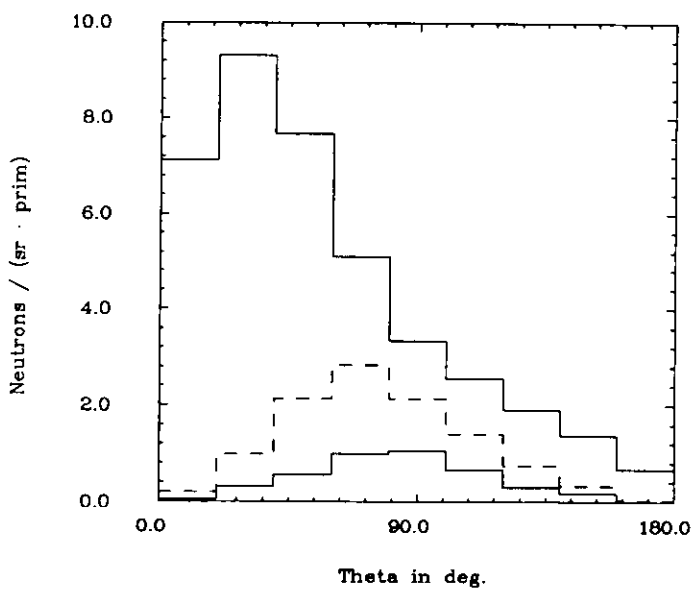

Figure 16: Angular distribution of high energy neutrons (energy intervall 14.9 to 400. MeV). Top graph: neutrons escaping the target; Middle (scale div. by 5): neutrons leaving 40 cm iron; Bottom (scale div. by 20): neutrons leaving 80 cm iron;

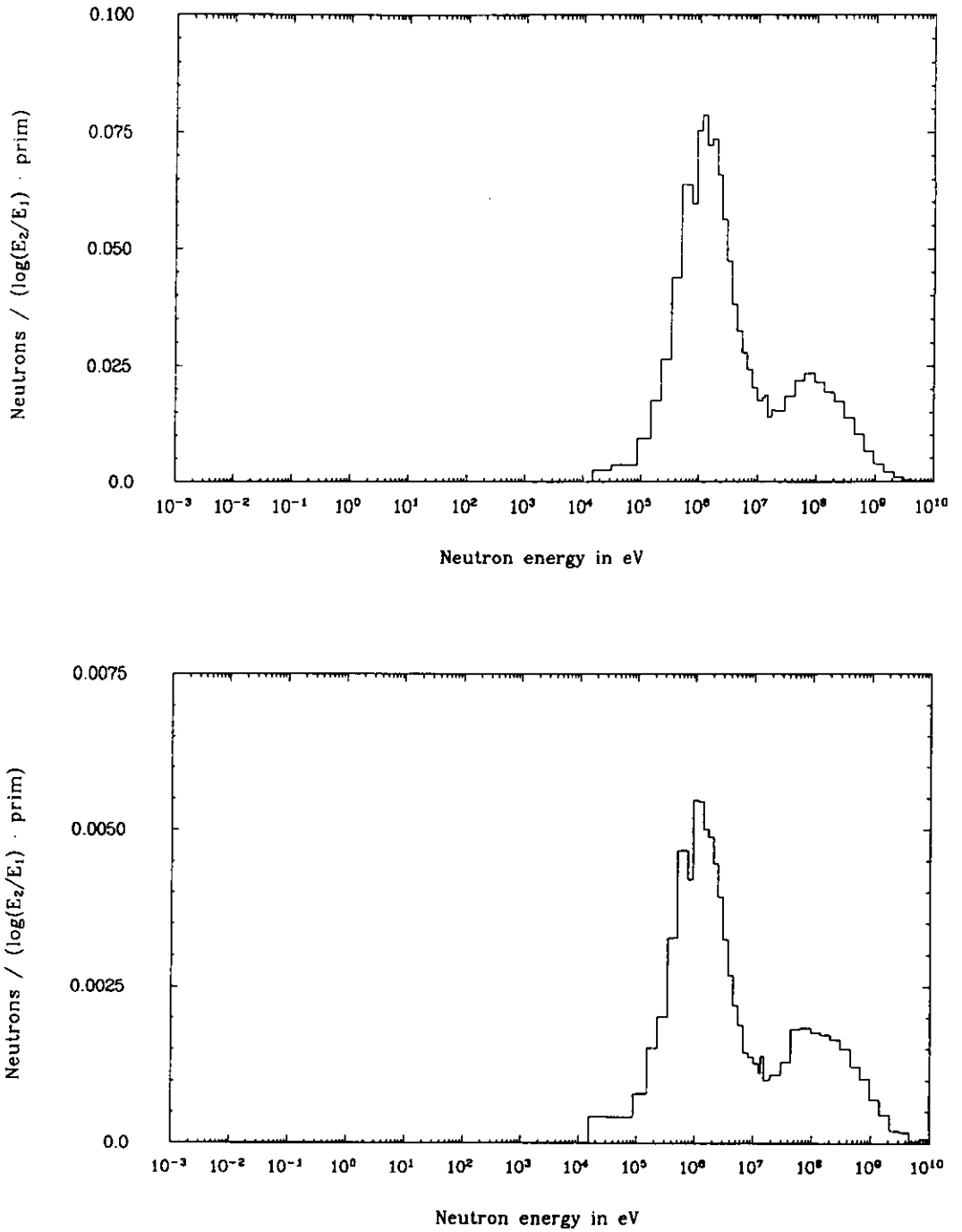

Figure 17: Fluence of neutrons entering the side shield. Top: Neutrons escaping the target between z = 0 ... 1 m; Bottom: Neutrons escaping the target between z = 1 ... 2 m;

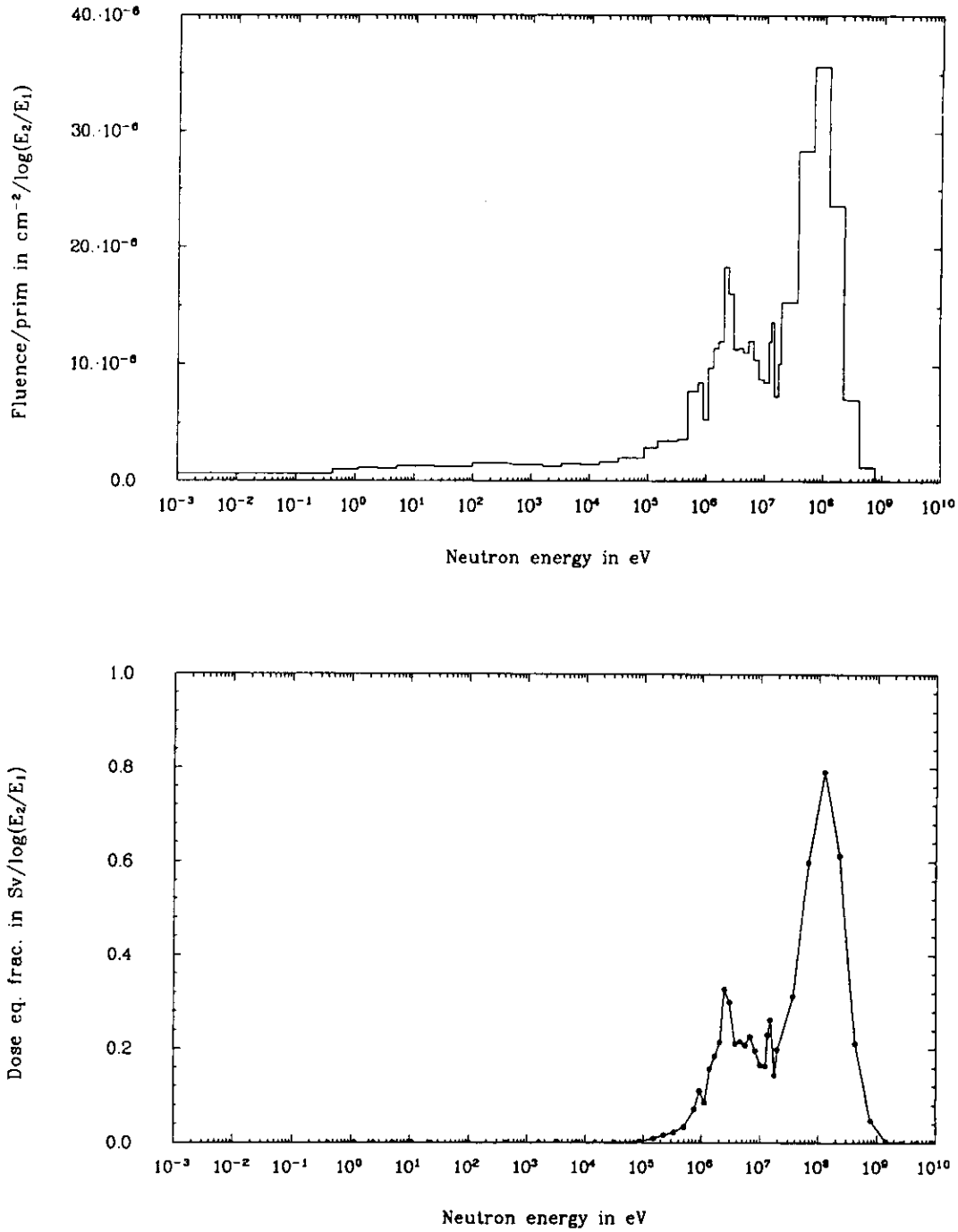

Figure 18: Fluence and dose equivalent spectrum behind 80 cm of concrete, registrated by detectors 2+3 and calculated by the boundary crossing estimator.

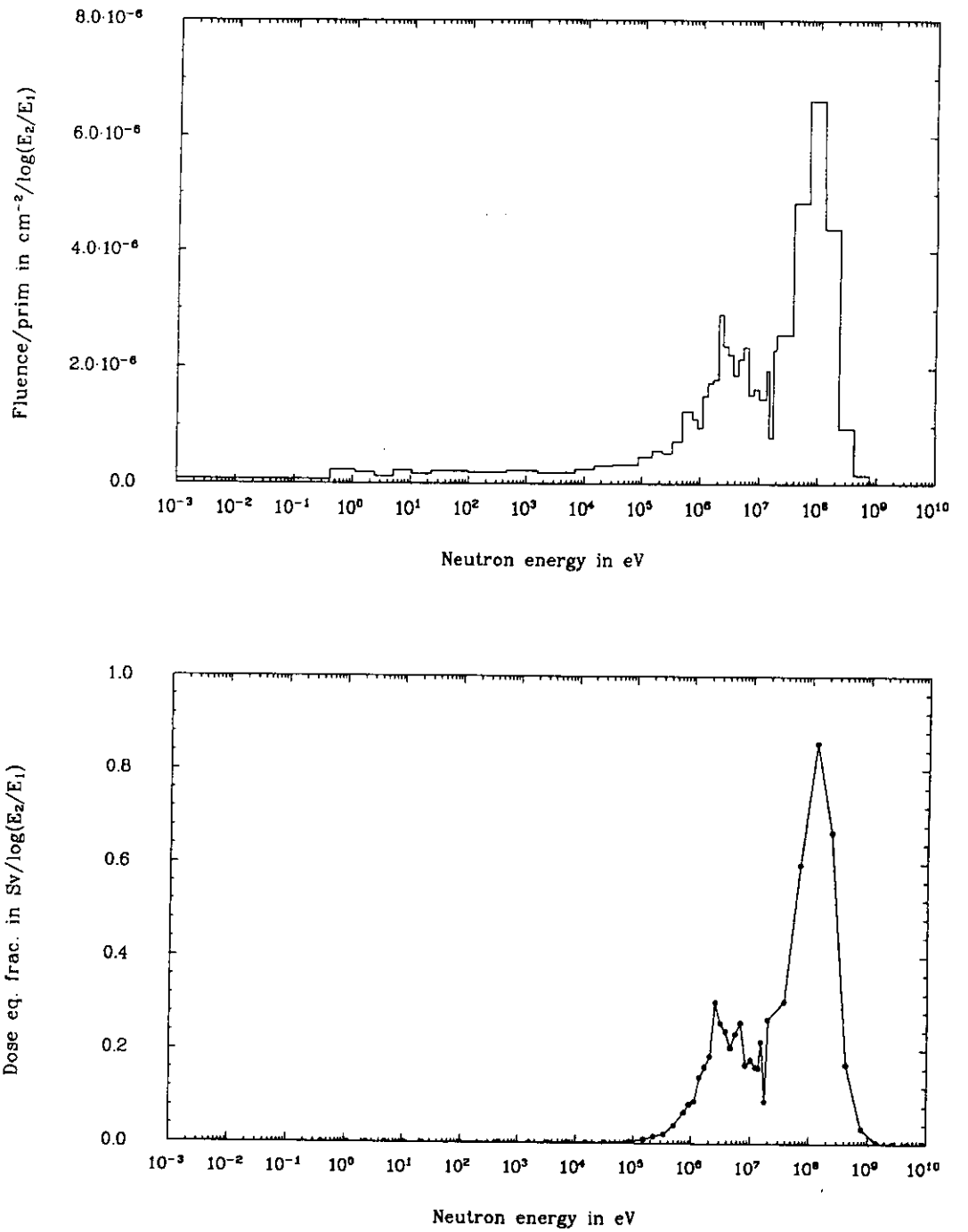

Figure 19: Fluence and dose equivalent spectrum behind 140 cm of concrete, registrated by detectors 2+3 and calculated by the boundary crossing estimator.

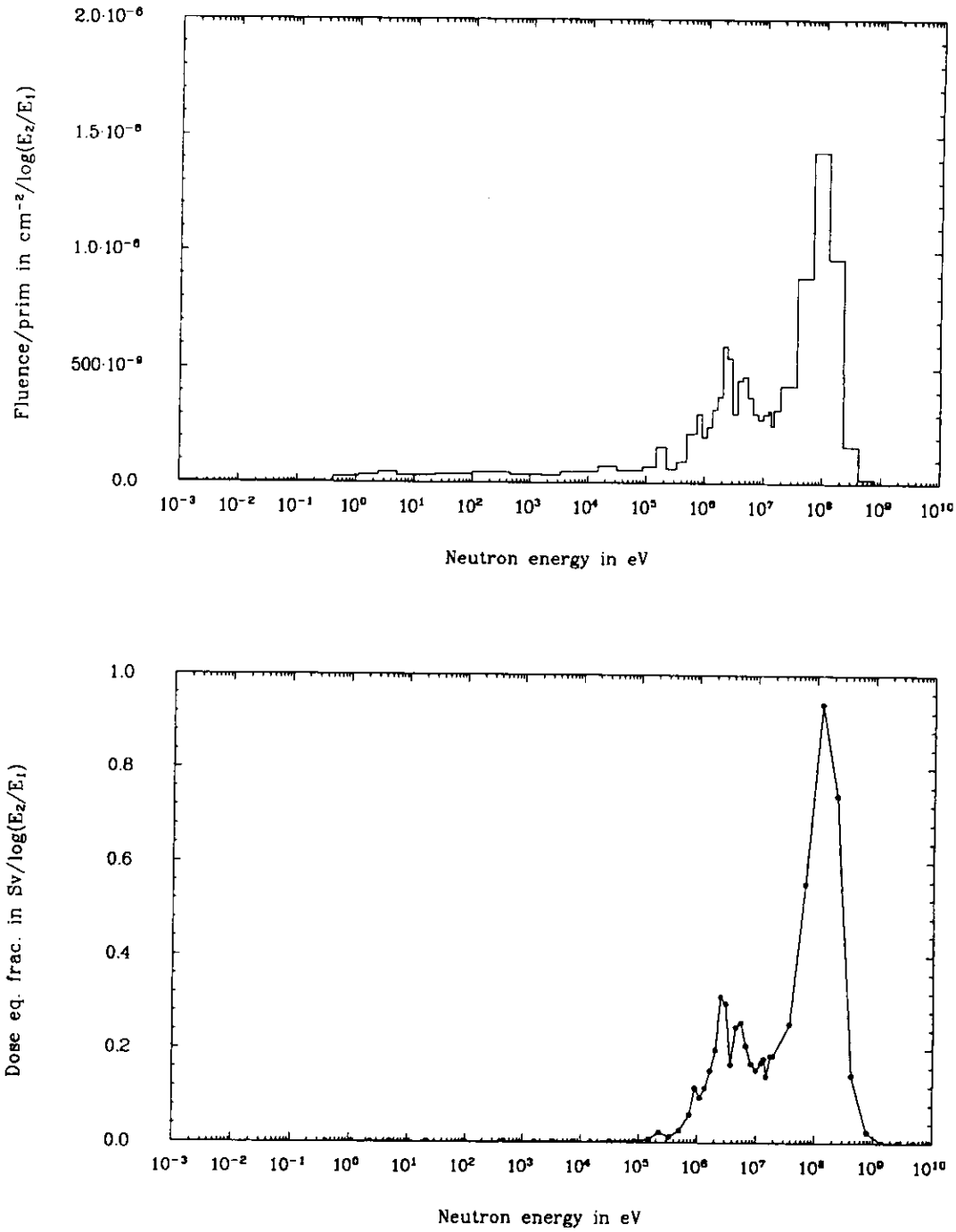

Figure 20: Fluence and dose equivalent spectrum behind 200 cm of concrete, registrated by detectors 2+3 and calculated by the boundary crossing estimator.

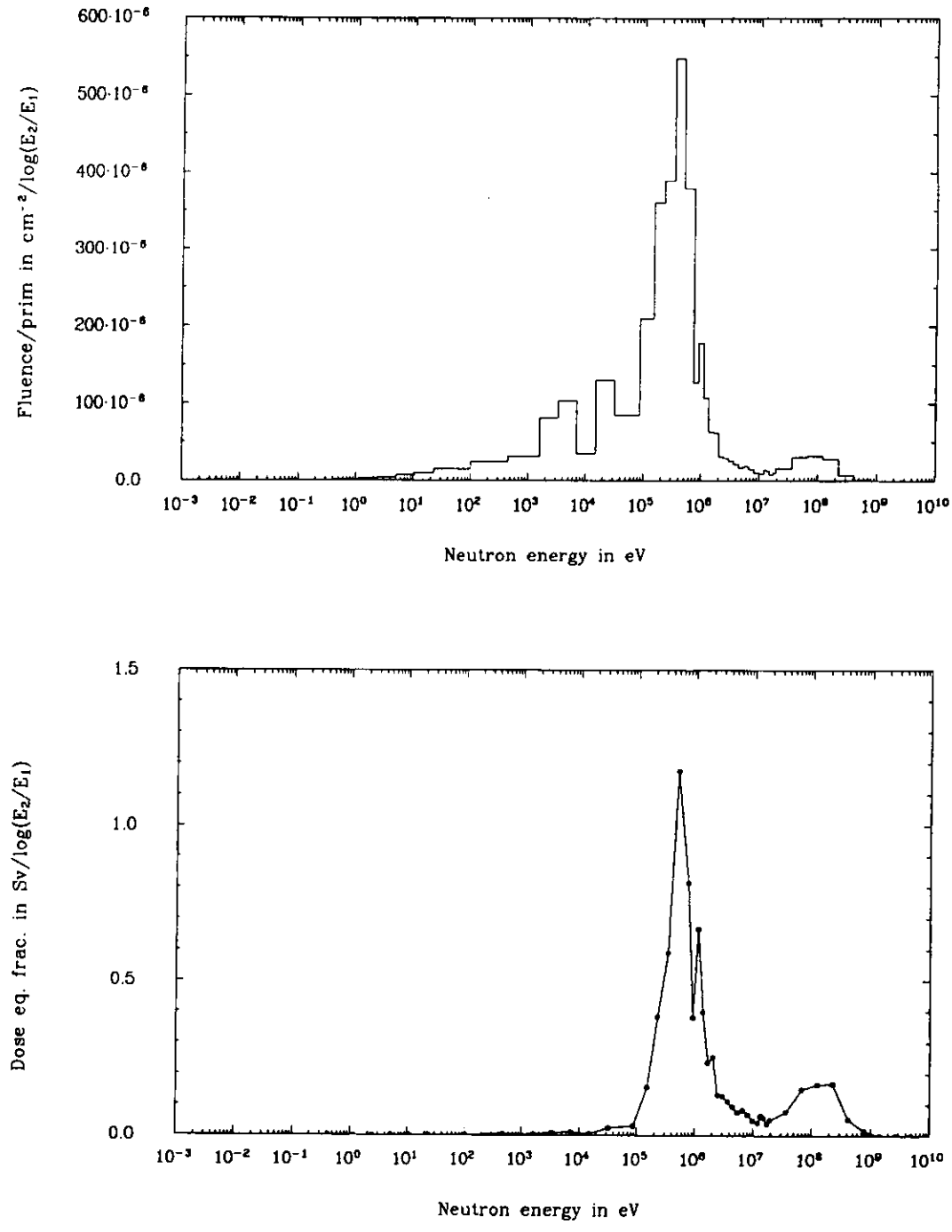

Figure 21: Fluence and dose equivalent spectrum behind 40 cm of iron, registrated by detectors 2+3 and calculated by the boundary crossing estimator.

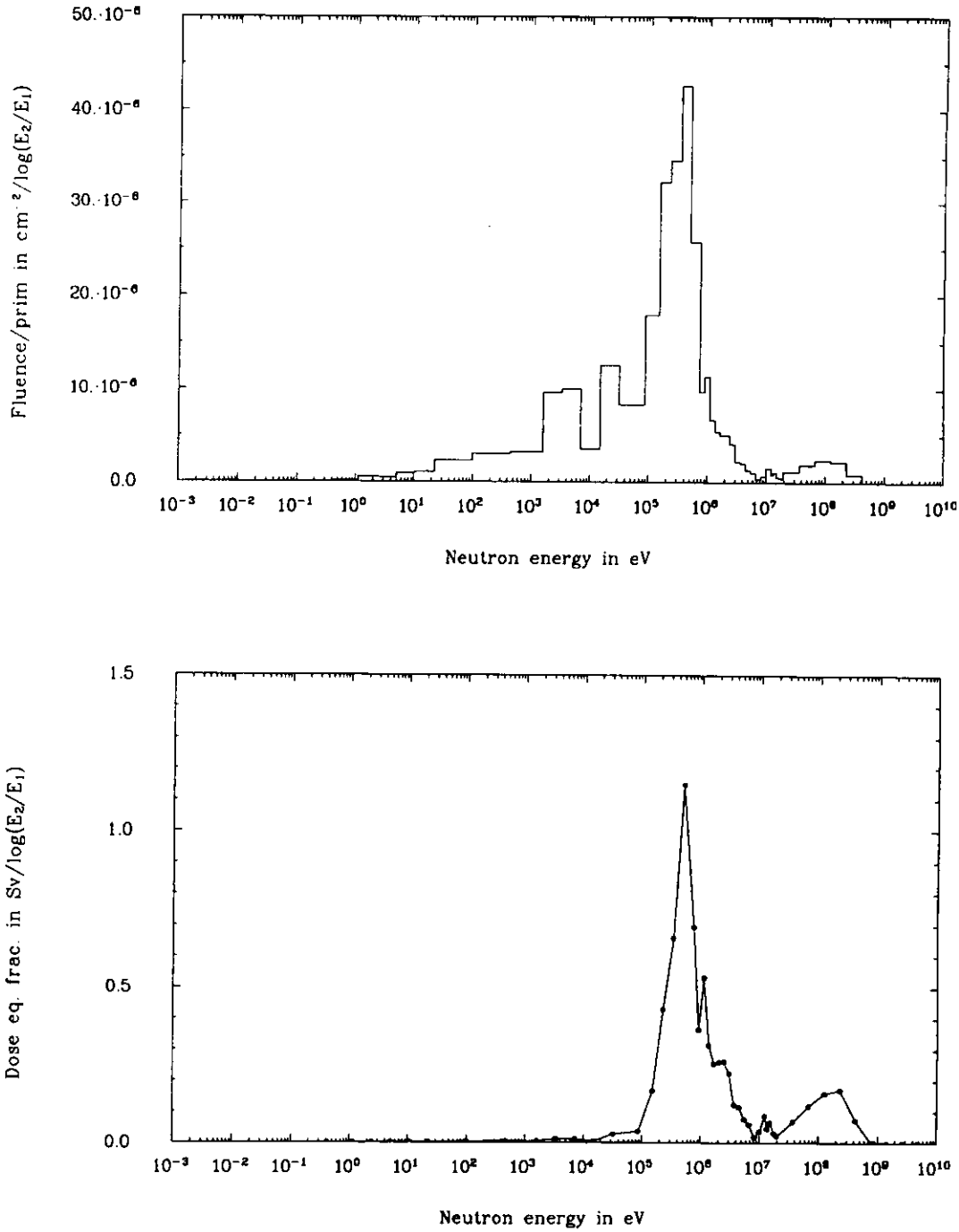

Figure 22: Fluence and dose equivalent spectrum behind 80 cm of iron, registrated by detectors 2+3 and calculated by the boundary crossing estimator.

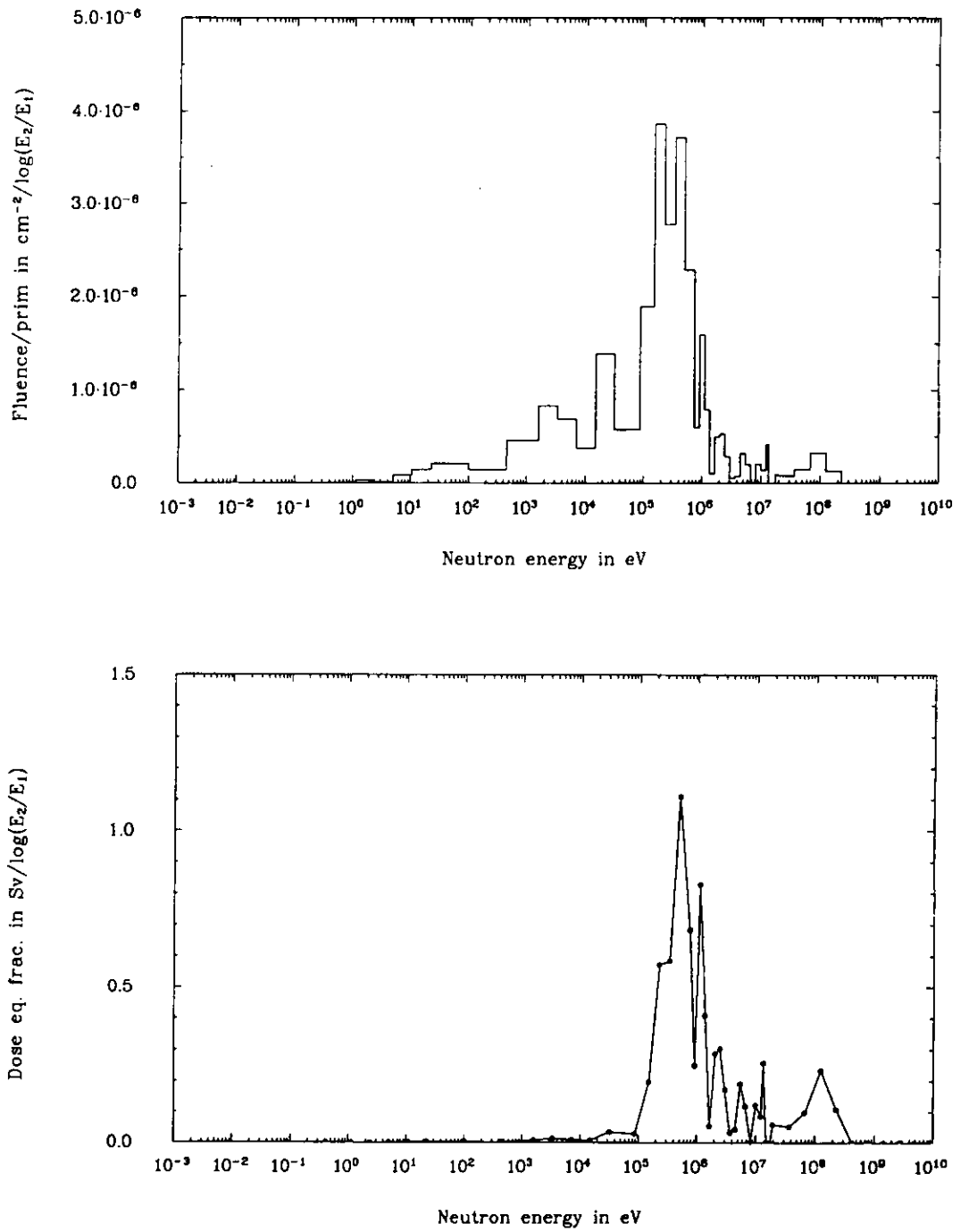

Figure 23: Fluence and dose equivalent spectrum behind 120 cm of iron, registrated by detectors 2+3 and calculated by the boundary crossing estimator.

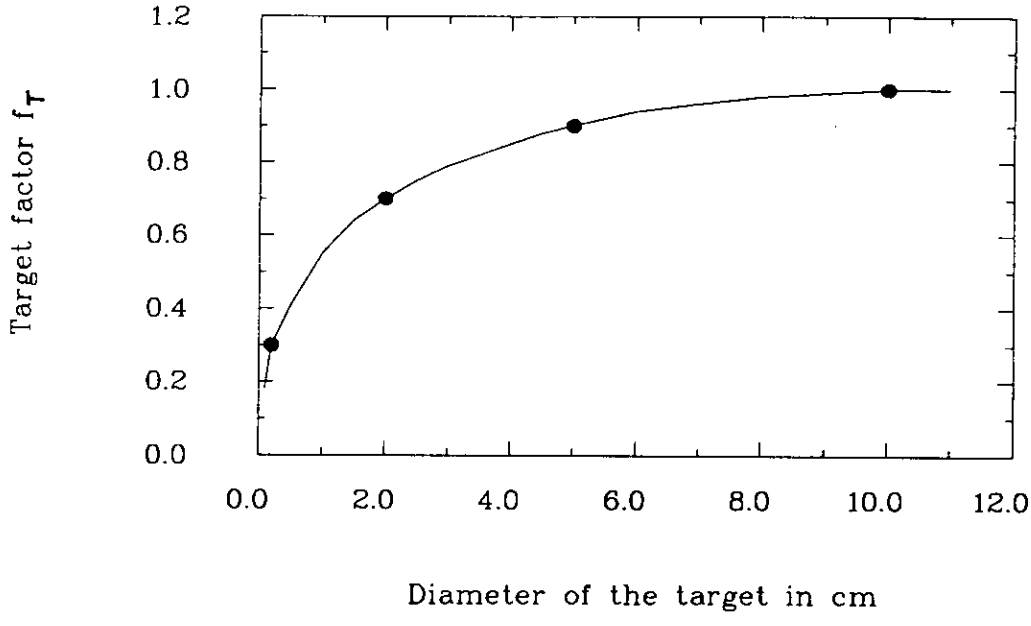

Figure 24: Dependence of the dose equivalent on the target diameter. The solid points are calculated values, the line is for interpolation and eye-guide.

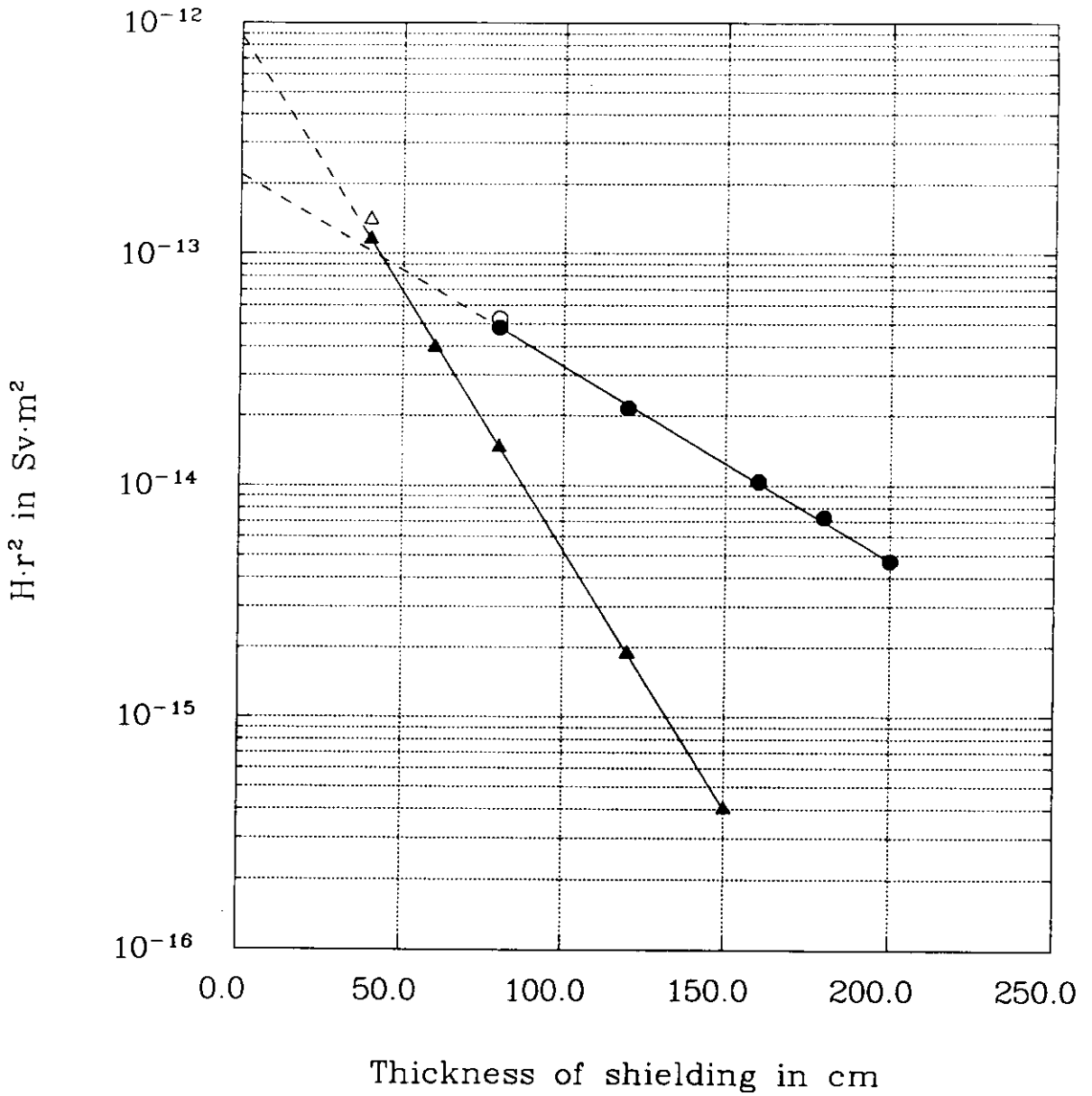

Figure 25: Attenuation of the dose equivalent in shielding material. The solid symbols (circles: concrete; triangles: iron) are calculated values for detectors 2+3. The open symbols represent experimental data.

Appendix

Comments to the following tables

Column	Subject
1	Number of energy group
2	Lower bin limits in eV
3	Upper bin limits in eV
4	Fluence spectrum in $n/(cm^2 \cdot eV)$
5	Fluence spectrum normalized to 1 beam particle in units $n/(cm^2 \cdot eV)$ (col. 4 $\approx$ col. 5)
6	Integral fluence spectrum (accumulated bins of col. 5)
7	Spectrum of dose equivalent, normalized to a total dose of 1 Sv, in units of Sv
8	Integral dose equivalent spectrum (accumulated bins of col. 7)

Fluences are calculated with the boundary crossing estimator.
Dose equivalents are calculated with conversion coefficients of ICRP21.
Fluences and doses are mean values of detectors 2+3 (Fig. 1).
OCONC means 'ordinary concrete'.

DSTOC5: STGEOM; OCONC; BDX, FLUENCE; D=80CM, DET.2+3, 120MIN

1	2	3	4	5	6	7	8
GRP NO.	LOW BINLIM EV	UPP BINLIM EV	FL-SP INPUT 1/(CM2*EV)	FL-SP NORM. 1/(CM2*EV)	FL-SP NORM. INTEGR.	DE-SP NORM. 1 SV	DE-SP NORM. INTEGR.
1	1.0000E-04	4.1400E-01	5.4999E-06	5.5029E-06	3.8670E-02	5.3521E-04	5.3521E-04
2	4.1400E-01	1.1254E+00	6.2033E-07	6.2067E-07	4.6167E-02	2.5430E-04	7.8951E-04
3	1.1254E+00	2.3824E+00	3.0109E-07	3.0126E-07	5.2596E-02	2.1722E-04	1.0067E-03
4	2.3824E+00	5.0435E+00	1.3504E-07	1.3512E-07	5.8700E-02	2.0460E-04	1.2113E-03
5	5.0435E+00	1.0677E+01	7.6651E-08	7.6693E-08	6.6036E-02	2.4187E-04	1.4532E-03
6	1.0677E+01	2.2603E+01	3.5664E-08	3.5683E-08	7.3261E-02	2.3627E-04	1.6895E-03
7	2.2603E+01	1.0130E+02	1.0466E-08	1.0471E-08	8.7252E-02	4.4613E-04	2.1356E-03
8	1.0130E+02	4.5400E+02	2.8375E-09	2.8390E-09	1.0425E-01	5.1441E-04	2.6500E-03
9	4.5400E+02	1.5846E+03	6.9715E-10	6.9753E-10	1.1764E-01	3.7789E-04	3.0279E-03
10	1.5846E+03	3.3546E+03	2.3600E-10	2.3613E-10	1.2474E-01	1.8352E-04	3.2114E-03
11	3.3546E+03	7.1018E+03	1.3343E-10	1.3351E-10	1.3323E-01	2.1390E-04	3.4253E-03
12	7.1018E+03	1.5034E+04	6.0073E-11	6.0105E-11	1.4133E-01	2.6053E-04	3.6858E-03
13	1.5034E+04	3.1828E+04	3.2349E-11	3.2366E-11	1.5055E-01	4.1574E-04	4.1016E-03
14	3.1828E+04	8.6517E+04	1.6188E-11	1.6197E-11	1.6559E-01	1.3693E-03	5.4708E-03
15	8.6517E+04	1.4996E+05	1.1079E-11	1.1085E-11	1.7753E-01	2.2714E-03	7.7422E-03
16	1.4996E+05	2.2371E+05	8.2077E-12	8.2122E-12	1.8781E-01	2.7807E-03	1.0523E-02
17	2.2371E+05	3.3373E+05	5.5563E-12	5.5593E-12	1.9820E-01	4.0017E-03	1.4525E-02
18	3.3373E+05	4.9787E+05	3.8659E-12	3.8680E-12	2.0898E-01	5.8797E-03	2.0404E-02
19	4.9787E+05	7.4274E+05	5.4988E-12	5.5018E-12	2.3185E-01	1.2477E-02	3.2881E-02
20	7.4274E+05	9.0718E+05	4.4963E-12	4.4987E-12	2.4441E-01	9.5778E-03	4.2459E-02
21	9.0718E+05	1.1080E+06	2.2931E-12	2.2943E-12	2.5223E-01	7.4195E-03	4.9878E-02
22	1.1080E+06	1.3534E+06	3.4649E-12	3.4668E-12	2.6668E-01	1.3700E-02	6.3578E-02
23	1.3534E+06	1.6530E+06	3.3234E-12	3.3252E-12	2.8359E-01	1.6042E-02	7.9620E-02
24	1.6530E+06	2.0190E+06	2.8607E-12	2.8622E-12	3.0138E-01	1.8631E-02	9.8251E-02
25	2.0190E+06	2.4660E+06	3.5757E-12	3.5776E-12	3.2853E-01	2.8442E-02	1.2669E-01
26	2.4660E+06	3.0119E+06	2.5634E-12	2.5647E-12	3.5230E-01	2.5997E-02	1.5269E-01
27	3.0119E+06	3.6788E+06	1.4788E-12	1.4796E-12	3.6905E-01	1.8322E-02	1.7101E-01
28	3.6788E+06	4.4933E+06	1.2238E-12	1.2244E-12	3.8598E-01	1.8702E-02	1.8971E-01
29	4.4933E+06	5.4881E+06	9.6820E-13	9.6873E-13	4.0235E-01	1.8071E-02	2.0779E-01
30	5.4881E+06	6.7032E+06	8.6469E-13	8.6516E-13	4.2019E-01	1.9714E-02	2.2750E-01
31	6.7032E+06	8.1873E+06	6.1225E-13	6.1258E-13	4.3563E-01	1.7111E-02	2.4461E-01
32	8.1873E+06	1.0000E+07	4.2190E-13	4.2213E-13	4.4862E-01	1.4402E-02	2.5901E-01
33	1.0000E+07	1.2214E+07	3.3447E-13	3.3465E-13	4.6120E-01	1.4167E-02	2.7318E-01
34	1.2214E+07	1.3499E+07	4.0638E-13	4.0660E-13	4.7007E-01	9.9903E-03	2.8317E-01
35	1.3499E+07	1.4918E+07	4.1957E-13	4.1980E-13	4.8018E-01	1.1390E-02	2.9456E-01
36	1.4918E+07	1.7500E+07	1.9655E-13	1.9666E-13	4.8880E-01	1.0001E-02	3.0456E-01
37	1.7500E+07	1.9600E+07	2.3737E-13	2.3750E-13	4.9727E-01	9.8238E-03	3.1438E-01
38	1.9600E+07	3.6802E+07	2.4452E-13	2.4466E-13	5.6872E-01	8.5514E-02	3.9990E-01
39	3.6802E+07	6.7719E+07	2.4268E-13	2.4281E-13	6.9618E-01	1.5859E-01	5.5848E-01
40	6.7719E+07	1.2461E+08	1.6570E-13	1.6579E-13	8.5632E-01	2.0968E-01	7.6817E-01
41	1.2461E+08	2.2930E+08	5.9646E-14	5.9678E-14	9.6238E-01	1.6235E-01	9.3052E-01
42	2.2930E+08	4.2193E+08	9.7058E-15	9.7111E-15	9.9414E-01	5.6023E-02	9.8654E-01
43	4.2193E+08	7.7639E+08	9.2987E-16	9.3038E-16	9.9974E-01	1.2460E-02	9.9900E-01
44	7.7639E+08	1.4286E+09	2.3340E-17	2.3353E-17	1.0000E+00	1.0001E-03	1.0000E+00
45	1.4286E+09	2.6288E+09	0.0000E+00	0.0000E+00	1.0000E+00	0.0000E+00	1.0000E+00
46	2.6288E+09	4.8373E+09	0.0000E+00	0.0000E+00	1.0000E+00	0.0000E+00	1.0000E+00

DSTOC5: STGEOM; OCONC; BDX, FLUENCE; D = 140CM, DET.2+3; 120MIN

1	2	3	4	5	6	7	8
GRP NO.	LOW BINLIM EV	UPP BINLIM EV	FL-SP INPUT 1/(CM2*EV)	FL-SP NORM. 1/(CM2*EV)	FL-SP NORM. INTEGR.	DE-SP NORM. 1 SV	DE-SP NORM. INTEGR.
1	1.0000E-04	4.1400E-01	6.4290E-07	6.4285E-07	2.7095E-02	3.6496E-04	3.6496E-04
2	4.1400E-01	1.1254E+00	1.4040E-07	1.4039E-07	3.7266E-02	3.3575E-04	7.0071E-04
3	1.1254E+00	2.3824E+00	4.9394E-08	4.9390E-08	4.3588E-02	2.0788E-04	9.0860E-04
4	2.3824E+00	5.0435E+00	1.5011E-08	1.5010E-08	4.7655E-02	1.3267E-04	1.0413E-03
5	5.0435E+00	1.0677E+01	1.3398E-08	1.3397E-08	5.5340E-02	2.4661E-04	1.2879E-03
6	1.0677E+01	2.2603E+01	4.5407E-09	4.5403E-09	6.0855E-02	1.7548E-04	1.4634E-03
7	2.2603E+01	1.0130E+02	1.7775E-09	1.7774E-09	7.5098E-02	4.4202E-04	1.9054E-03
8	1.0130E+02	4.5400E+02	3.5639E-10	3.5636E-10	8.7897E-02	3.7691E-04	2.2823E-03
9	4.5400E+02	1.5846E+03	1.0901E-10	1.0901E-10	1.0045E-01	3.4472E-04	2.6270E-03
10	1.5846E+03	3.3546E+03	3.3809E-11	3.3807E-11	1.0654E-01	1.5337E-04	2.7804E-03
11	3.3546E+03	7.1018E+03	1.6496E-11	1.6495E-11	1.1284E-01	1.5427E-04	2.9346E-03
12	7.1018E+03	1.5034E+04	1.0177E-11	1.0176E-11	1.2106E-01	2.5747E-04	3.1921E-03
13	1.5034E+04	3.1828E+04	6.0196E-12	6.0192E-12	1.3135E-01	4.5130E-04	3.6434E-03
14	3.1828E+04	8.6517E+04	2.5887E-12	2.5885E-12	1.4576E-01	1.2774E-03	4.9208E-03
15	8.6517E+04	1.4996E+05	1.7513E-12	1.7512E-12	1.5708E-01	2.0946E-03	7.0154E-03
16	1.4996E+05	2.2371E+05	1.3293E-12	1.3292E-12	1.6706E-01	2.6273E-03	9.6427E-03
17	2.2371E+05	3.3373E+05	8.3386E-13	8.3380E-13	1.7640E-01	3.5034E-03	1.3146E-02
18	3.3373E+05	4.9787E+05	7.7199E-13	7.7193E-13	1.8931E-01	6.8495E-03	1.9996E-02
19	4.9787E+05	7.4274E+05	8.8613E-13	8.8607E-13	2.1140E-01	1.1729E-02	3.1725E-02
20	7.4274E+05	9.0718E+05	5.9107E-13	5.9103E-13	2.2130E-01	7.3450E-03	3.9070E-02
21	9.0718E+05	1.1080E+06	4.1778E-13	4.1775E-13	2.2984E-01	7.8856E-03	4.6955E-02
22	1.1080E+06	1.3534E+06	5.3524E-13	5.3520E-13	2.4321E-01	1.2345E-02	5.9301E-02
23	1.3534E+06	1.6530E+06	5.0535E-13	5.0531E-13	2.5863E-01	1.4230E-02	7.3531E-02
24	1.6530E+06	2.0190E+06	4.2662E-13	4.2659E-13	2.7453E-01	1.6209E-02	8.9740E-02
25	2.0190E+06	2.4660E+06	5.6652E-13	5.6648E-13	3.0032E-01	2.6287E-02	1.1603E-01
26	2.4660E+06	3.0119E+06	3.7816E-13	3.7813E-13	3.2134E-01	2.2374E-02	1.3840E-01
27	3.0119E+06	3.6788E+06	2.8993E-13	2.8990E-13	3.4103E-01	2.0955E-02	1.5936E-01
28	3.6788E+06	4.4933E+06	1.9978E-13	1.9976E-13	3.5759E-01	1.7810E-02	1.7717E-01
29	4.4933E+06	5.4881E+06	1.8741E-13	1.8739E-13	3.7658E-01	2.0406E-02	1.9757E-01
30	5.4881E+06	6.7032E+06	1.6885E-13	1.6884E-13	3.9747E-01	2.2457E-02	2.2003E-01
31	6.7032E+06	8.1873E+06	8.9485E-14	8.9479E-14	4.1099E-01	1.4590E-02	2.3462E-01
32	8.1873E+06	1.0000E+07	7.8238E-14	7.8232E-14	4.2543E-01	1.5580E-02	2.5020E-01
33	1.0000E+07	1.2214E+07	5.7306E-14	5.7302E-14	4.3835E-01	1.4160E-02	2.6436E-01
34	1.2214E+07	1.3499E+07	4.9007E-14	4.9004E-14	4.4476E-01	7.0283E-03	2.7139E-01
35	1.3499E+07	1.4918E+07	5.9817E-14	5.9813E-14	4.5341E-01	9.4731E-03	2.8086E-01
36	1.4918E+07	1.7500E+07	2.1237E-14	2.1236E-14	4.5899E-01	6.3042E-03	2.8716E-01
37	1.7500E+07	1.9600E+07	5.4175E-14	5.4171E-14	4.7058E-01	1.3080E-02	3.0024E-01
38	1.9600E+07	3.6802E+07	4.0870E-14	4.0867E-14	5.4216E-01	8.3379E-02	3.8362E-01
39	3.6802E+07	6.7719E+07	4.1489E-14	4.1486E-14	6.7278E-01	1.5817E-01	5.4179E-01
40	6.7719E+07	1.2461E+08	3.0769E-14	3.0766E-14	8.5102E-01	2.2714E-01	7.6892E-01
41	1.2461E+08	2.2930E+08	1.1126E-14	1.1125E-14	9.6962E-01	1.7667E-01	9.4559E-01
42	2.2930E+08	4.2193E+08	1.3304E-15	1.3303E-15	9.9572E-01	4.4797E-02	9.9039E-01
43	4.2193E+08	7.7639E+08	1.1291E-16	1.1290E-16	9.9979E-01	8.8254E-03	9.9921E-01
44	7.7639E+08	1.4286E+09	3.1604E-18	3.1602E-18	1.0000E+00	7.8996E-04	1.0000E+00
45	1.4286E+09	2.6288E+09	0.0000E+00	0.0000E+00	1.0000E+00	0.0000E+00	1.0000E+00

DSTOC5: STGEOM; OCONC; BDX, FLUENCE; D=200CM, DET.2+3; 225MIN

1	2	3	4	5	6	7	8
GRP NO.	LOW BINLIM EV	UPP BINLIM EV	FL-SP INPUT 1/(CM2*EV)	FL-SP NORM. 1/(CM2*EV)	FL-SP NORM. INTEGR.	DE-SP NORM. 1 SV	DE-SP NORM. INTEGR.
1	1.0000E-04	4.1400E-01	4.6437E-08	4.6464E-08	1.0175E-02	1.3337E-04	1.3337E-04
2	4.1400E-01	1.1254E+00	1.6802E-08	1.6812E-08	1.6503E-02	2.0329E-04	3.3665E-04
3	1.1254E+00	2.3824E+00	9.0557E-09	9.0610E-09	2.2530E-02	1.9282E-04	5.2947E-04
4	2.3824E+00	5.0435E+00	5.6505E-09	5.6538E-09	3.0490E-02	2.5266E-04	7.8213E-04
5	5.0435E+00	1.0677E+01	1.8390E-09	1.8400E-09	3.5975E-02	1.7126E-04	9.5338E-04
6	1.0677E+01	2.2603E+01	8.5208E-10	8.5257E-10	4.1355E-02	1.6660E-04	1.1200E-03
7	2.2603E+01	1.0130E+02	3.0177E-10	3.0194E-10	5.3927E-02	3.7965E-04	1.4996E-03
8	1.0130E+02	4.5400E+02	8.3748E-11	8.3797E-11	6.9565E-02	4.4810E-04	1.9477E-03
9	4.5400E+02	1.5846E+03	1.7793E-11	1.7804E-11	8.0215E-02	2.8466E-04	2.2324E-03
10	1.5846E+03	3.3546E+03	6.2467E-12	6.2503E-12	8.6068E-02	1.4336E-04	2.3758E-03
11	3.3546E+03	7.1018E+03	4.2029E-12	4.2053E-12	9.4406E-02	1.9885E-04	2.5746E-03
12	7.1018E+03	1.5034E+04	2.0568E-12	2.0580E-12	1.0304E-01	2.6326E-04	2.8379E-03
13	1.5034E+04	3.1828E+04	1.4028E-12	1.4037E-12	1.1552E-01	5.3209E-04	3.3700E-03
14	3.1828E+04	6.6517E+04	4.4349E-13	4.4375E-13	1.2836E-01	1.1071E-03	4.4771E-03
15	6.6517E+04	1.4996E+05	2.5990E-13	2.6005E-13	1.3709E-01	1.5726E-03	6.0497E-03
16	1.4996E+05	2.2371E+05	3.7385E-13	3.7407E-13	1.5168E-01	3.7381E-03	9.7878E-03
17	2.2371E+05	3.3373E+05	9.9275E-14	9.9333E-14	1.5746E-01	2.1102E-03	1.1898E-02
18	3.3373E+05	4.9787E+05	9.8528E-14	9.8586E-14	1.6603E-01	4.4227E-03	1.6321E-02
19	4.9787E+05	7.4274E+05	1.5489E-13	1.5498E-13	1.8610E-01	1.0372E-02	2.6693E-02
20	7.4274E+05	9.0718E+05	1.6076E-13	1.6085E-13	2.0010E-01	1.0107E-02	3.6799E-02
21	9.0718E+05	1.1080E+06	8.7542E-14	8.7593E-14	2.0941E-01	8.3597E-03	4.5159E-02
22	1.1080E+06	1.3534E+06	8.7216E-14	8.7267E-14	2.2074E-01	1.0177E-02	5.5336E-02
23	1.3534E+06	1.6530E+06	9.3610E-14	9.3664E-14	2.3559E-01	1.3336E-02	6.8672E-02
24	1.6530E+06	2.0190E+06	8.9399E-14	8.9451E-14	2.5291E-01	1.7184E-02	8.5856E-02
25	2.0190E+06	2.4660E+06	1.1548E-13	1.1554E-13	2.8023E-01	2.7108E-02	1.1296E-01
26	2.4660E+06	3.0119E+06	8.6423E-14	8.6474E-14	3.0521E-01	2.5868E-02	1.3883E-01
27	3.0119E+06	3.6788E+06	3.9629E-14	3.9652E-14	3.1920E-01	1.4491E-02	1.5332E-01
28	3.6788E+06	4.4933E+06	4.7583E-14	4.7610E-14	3.3972E-01	2.1461E-02	1.7479E-01
29	4.4933E+06	5.4881E+06	4.0497E-14	4.0520E-14	3.6105E-01	2.2308E-02	1.9709E-01
30	5.4881E+06	6.7032E+06	2.6780E-14	2.6796E-14	3.7828E-01	1.8019E-02	2.1511E-01
31	6.7032E+06	8.1873E+06	1.7806E-14	1.7817E-14	3.9227E-01	1.4687E-02	2.2980E-01
32	8.1873E+06	1.0000E+07	1.3380E-14	1.3388E-14	4.0511E-01	1.3480E-02	2.4328E-01
33	1.0000E+07	1.2214E+07	1.1828E-14	1.1834E-14	4.1897E-01	1.4786E-02	2.5807E-01
34	1.2214E+07	1.3499E+07	1.0721E-14	1.0727E-14	4.2626E-01	7.7783E-03	2.6584E-01
35	1.3499E+07	1.4918E+07	7.7182E-15	7.7227E-15	4.3206E-01	6.1839E-03	2.7203E-01
36	1.4918E+07	1.7500E+07	8.5750E-15	8.5800E-15	4.4378E-01	1.2878E-02	2.8491E-01
37	1.7500E+07	1.9600E+07	7.4942E-15	7.4985E-15	4.5211E-01	9.1537E-03	2.9406E-01
38	1.9600E+07	3.6802E+07	6.7358E-15	6.7397E-15	5.1346E-01	6.9522E-02	3.6358E-01
39	3.6802E+07	6.7719E+07	7.6164E-15	7.6208E-15	6.3812E-01	1.4690E-01	5.1048E-01
40	6.7719E+07	1.2461E+08	6.6543E-15	6.6581E-15	8.3854E-01	2.4852E-01	7.5899E-01
41	1.2461E+08	2.2930E+08	2.4477E-15	2.4491E-15	9.7419E-01	1.9663E-01	9.5562E-01
42	2.2930E+08	4.2193E+08	2.2469E-16	2.2482E-16	9.9710E-01	3.8277E-02	9.9389E-01
43	4.2193E+08	7.7639E+08	1.5438E-17	1.5447E-17	1.0000E+00	6.1049E-03	1.0000E+00
44	7.7639E+08	1.4286E+09	0.0000E+00	0.0000E+00	1.0000E+00	0.0000E+00	1.0000E+00
45	1.4286E+09	2.6288E+09	0.0000E+00	0.0000E+00	1.0000E+00	0.0000E+00	1.0000E+00
46	2.6288E+09	4.8373E+09	0.0000E+00	0.0000E+00	1.0000E+00	0.0000E+00	1.0000E+00
47	4.8373E+09	8.9011E+09	0.0000E+00	0.0000E+00	1.0000E+00	0.0000E+00	1.0000E+00

DSTFE5: STGEOM; IRON; BDX, FLUENCE; D = 40CM, DET.2+3; 30MIN

1	2	3	4	5	6	7	8
GRP NO.	LOW BINLIM EV	UPP BINLIM EV	FL-SP INPUT 1/(CM2*EV)	FL-SP NORM. 1/(CM2*EV)	FL-SP NORM. INTEGR.	DE-SP NORM. 1 SV	DE-SP NORM. INTEGR.
1	1.0000E-04	4.1400E-01	0.0000E+00	0.0000E+00	0.0000E+00	0.0000E+00	0.0000E+00
2	4.1400E-01	1.1254E+00	8.7158E-07	8.7148E-07	9.7022E-04	8.2804E-05	8.2804E-05
3	1.1254E+00	2.3824E+00	7.1202E-07	7.1194E-07	2.3707E-03	1.1905E-04	2.0185E-04
4	2.3824E+00	5.0435E+00	5.6479E-07	5.6472E-07	4.7224E-03	1.9830E-04	4.0016E-04
5	5.0435E+00	1.0677E+01	4.2782E-07	4.2777E-07	8.4937E-03	3.1285E-04	7.1300E-04
6	1.0677E+01	2.2603E+01	2.7084E-07	2.7081E-07	1.3548E-02	4.1583E-04	1.1288E-03
7	2.2603E+01	1.0130E+02	1.2849E-07	1.2847E-07	2.9370E-02	1.2693E-03	2.3982E-03
8	1.0130E+02	4.5400E+02	4.4701E-08	4.4696E-08	5.4040E-02	1.8781E-03	4.2763E-03
9	4.5400E+02	1.5846E+03	1.5206E-08	1.5204E-08	8.0942E-02	1.9102E-03	6.1865E-03
10	1.5846E+03	3.3546E+03	1.4943E-08	1.4941E-08	1.2233E-01	2.6930E-03	8.8794E-03
11	3.3546E+03	7.1018E+03	8.9577E-09	8.9566E-09	1.7485E-01	3.3279E-03	1.2207E-02
12	7.1018E+03	1.5034E+04	1.4409E-09	1.4407E-09	1.9274E-01	1.4482E-03	1.3656E-02
13	1.5034E+04	3.1828E+04	2.5234E-09	2.5231E-09	2.5905E-01	7.5157E-03	2.1171E-02
14	3.1828E+04	8.6517E+04	6.7269E-10	6.7261E-10	3.1661E-01	1.3186E-02	3.4358E-02
15	8.6517E+04	1.4996E+05	7.8877E-10	7.8867E-10	3.9492E-01	3.7477E-02	7.1835E-02
16	1.4996E+05	2.2371E+05	8.4789E-10	8.4779E-10	4.9276E-01	6.6573E-02	1.3841E-01
17	2.2371E+05	3.3373E+05	6.1391E-10	6.1384E-10	5.9845E-01	1.0247E-01	2.4088E-01
18	3.3373E+05	4.9787E+05	5.7974E-10	5.7967E-10	7.4735E-01	2.0434E-01	4.4522E-01
19	4.9787E+05	7.4274E+05	2.6891E-10	2.6888E-10	8.5039E-01	1.4141E-01	5.8663E-01
20	7.4274E+05	9.0718E+05	6.6927E-11	6.6919E-11	8.6761E-01	3.3040E-02	6.1966E-01
21	9.0718E+05	1.1080E+06	7.7186E-11	7.7177E-11	8.9186E-01	5.7878E-02	6.7754E-01
22	1.1080E+06	1.3534E+06	3.7814E-11	3.7810E-11	9.0639E-01	3.4650E-02	7.1219E-01
23	1.3534E+06	1.6530E+06	1.8308E-11	1.8306E-11	9.1497E-01	2.0481E-02	7.3267E-01
24	1.6530E+06	2.0190E+06	1.4615E-11	1.4613E-11	9.2334E-01	2.2059E-02	7.5473E-01
25	2.0190E+06	2.4660E+06	6.2102E-12	6.2095E-12	9.2768E-01	1.1448E-02	7.6618E-01
26	2.4660E+06	3.0119E+06	4.7595E-12	4.7589E-12	9.3175E-01	1.1187E-02	7.7737E-01
27	3.0119E+06	3.6788E+06	3.3708E-12	3.3704E-12	9.3526E-01	9.6789E-03	7.8705E-01
28	3.6788E+06	4.4933E+06	2.2846E-12	2.2843E-12	9.3818E-01	8.0911E-03	7.9514E-01
29	4.4933E+06	5.4881E+06	1.4890E-12	1.4889E-12	9.4049E-01	6.4410E-03	8.0158E-01
30	5.4881E+06	6.7032E+06	1.3432E-12	1.3430E-12	9.4305E-01	7.0969E-03	8.0868E-01
31	6.7032E+06	8.1873E+06	9.0644E-13	9.0634E-13	9.4515E-01	5.8711E-03	8.1455E-01
32	8.1873E+06	1.0000E+07	5.2695E-13	5.2689E-13	9.4665E-01	4.1687E-03	8.1872E-01
33	1.0000E+07	1.2214E+07	3.6392E-13	3.6387E-13	9.4791E-01	3.5723E-03	8.2229E-01
34	1.2214E+07	1.3499E+07	4.8380E-13	4.8375E-13	9.4888E-01	2.7564E-03	8.2504E-01
35	1.3499E+07	1.4918E+07	4.0668E-13	4.0663E-13	9.4978E-01	2.5586E-03	8.2760E-01
36	1.4918E+07	1.7500E+07	2.2313E-13	2.2311E-13	9.5069E-01	2.6314E-03	8.3023E-01
37	1.7500E+07	1.9600E+07	2.5925E-13	2.5922E-13	9.5154E-01	2.4866E-03	8.3272E-01
38	1.9600E+07	3.6802E+07	2.6051E-13	2.6048E-13	9.5855E-01	2.1114E-02	8.5383E-01
39	3.6802E+07	6.7719E+07	2.6344E-13	2.6341E-13	9.7129E-01	3.9897E-02	8.9373E-01
40	6.7719E+07	1.2461E+08	1.4987E-13	1.4985E-13	9.8464E-01	4.3952E-02	9.3768E-01
41	1.2461E+08	2.2930E+08	7.0459E-14	7.0451E-14	9.9618E-01	4.4445E-02	9.8213E-01
42	2.2930E+08	4.2193E+08	1.0132E-14	1.0130E-14	9.9923E-01	1.3553E-02	9.9568E-01
43	4.2193E+08	7.7639E+08	1.3911E-15	1.3909E-15	1.0000E+00	4.3198E-03	1.0000E+00
44	7.7639E+08	1.4286E+09	0.0000E+00	0.0000E+00	1.0000E+00	0.0000E+00	1.0000E+00
45	1.4286E+09	2.6288E+09	0.0000E+00	0.0000E+00	1.0000E+00	0.0000E+00	1.0000E+00
46	2.6288E+09	4.8373E+09	0.0000E+00	0.0000E+00	1.0000E+00	0.0000E+00	1.0000E+00

DSTFE5: STGEOM; IRON; BDX, FLUENCE, D = 80CM, DET.2+3; 60MIN

1	2	3	4	5	6	7	8
GRP NO.	LOW BINLIM EV	UPP BINLIM EV	FL-SP INPUT 1/(CM2*EV)	FL-SP NORM. 1/(CM2*EV)	FL-SP NORM. INTEGR.	DE-SP NORM. 1 SV	DE-SP NORM. INTEGR.
1	1.0000E-04	4.1400E-01	0.0000E+00	0.0000E+00	0.0000E+00	0.0000E+00	0.0000E+00
2	4.1400E-01	1.1254E+00	6.9990E-08	7.0030E-08	8.7710E-04	8.3542E-05	8.3542E-05
3	1.1254E+00	2.3824E+00	1.4322E-07	1.4330E-07	4.0483E-03	3.0084E-04	3.8439E-04
4	2.3824E+00	5.0435E+00	6.0011E-08	6.0045E-08	6.8615E-03	2.6473E-04	6.4912E-04
5	5.0435E+00	1.0677E+01	5.5586E-08	5.5617E-08	1.2378E-02	5.1069E-04	1.1598E-03
6	1.0677E+01	2.2603E+01	2.9773E-08	2.9790E-08	1.8632E-02	5.7431E-04	1.7341E-03
7	2.2603E+01	1.0130E+02	1.9594E-08	1.9605E-08	4.5796E-02	2.4320E-03	4.1661E-03
8	1.0130E+02	4.5400E+02	5.5972E-09	5.6004E-09	8.0571E-02	2.9546E-03	7.1207E-03
9	4.5400E+02	1.5846E+03	1.5459E-09	1.5467E-09	1.1136E-01	2.4398E-03	9.5605E-03
10	1.5846E+03	3.3546E+03	1.7695E-09	1.7704E-09	1.6653E-01	4.0063E-03	1.3567E-02
11	3.3546E+03	7.1018E+03	8.7154E-10	8.7203E-10	2.2406E-01	4.0680E-03	1.7635E-02
12	7.1018E+03	1.5034E+04	1.4889E-10	1.4898E-10	2.4486E-01	1.8801E-03	1.9515E-02
13	1.5034E+04	3.1828E+04	2.4300E-10	2.4314E-10	3.1675E-01	9.0931E-03	2.8608E-02
14	3.1828E+04	8.6517E+04	6.5969E-11	6.6006E-11	3.8031E-01	1.6247E-02	4.4855E-02
15	8.6517E+04	1.4996E+05	6.7509E-11	6.7547E-11	4.5575E-01	4.0300E-02	8.5155E-02
16	1.4996E+05	2.2371E+05	7.5873E-11	7.5916E-11	5.5432E-01	7.4846E-02	1.6000E-01
17	2.2371E+05	3.3373E+05	5.4600E-11	5.4631E-11	6.6014E-01	1.1450E-01	2.7450E-01
18	3.3373E+05	4.9787E+05	4.5078E-11	4.5104E-11	7.9048E-01	1.9963E-01	4.7413E-01
19	4.9787E+05	7.4274E+05	1.8261E-11	1.8271E-11	8.6925E-01	1.2064E-01	5.9477E-01
20	7.4274E+05	9.0718E+05	5.1051E-12	5.1079E-12	8.8404E-01	3.1663E-02	6.2643E-01
21	9.0718E+05	1.1080E+06	4.9029E-12	4.9056E-12	9.0138E-01	4.6190E-02	6.7262E-01
22	1.1080E+06	1.3534E+06	2.3800E-12	2.3813E-12	9.1167E-01	2.7399E-02	7.0002E-01
23	1.3534E+06	1.6530E+06	1.5802E-12	1.5811E-12	9.2001E-01	2.2210E-02	7.2223E-01
24	1.6530E+06	2.0190E+06	1.1947E-12	1.1954E-12	9.2771E-01	2.2655E-02	7.4488E-01
25	2.0190E+06	2.4660E+06	9.8404E-13	9.8460E-13	9.3546E-01	2.2790E-02	7.6767E-01
26	2.4660E+06	3.0119E+06	6.6072E-13	6.6109E-13	9.4182E-01	1.9511E-02	7.8718E-01
27	3.0119E+06	3.6788E+06	2.9823E-13	2.9840E-13	9.4532E-01	1.0759E-02	7.9794E-01
28	3.6788E+06	4.4933E+06	2.2694E-13	2.2707E-13	9.4857E-01	1.0098E-02	8.0804E-01
29	4.4933E+06	5.4881E+06	1.2139E-13	1.2146E-13	9.5070E-01	6.5973E-03	8.1464E-01
30	5.4881E+06	6.7032E+06	7.7769E-14	7.7813E-14	9.5237E-01	5.1624E-03	8.1980E-01
31	6.7032E+06	8.1873E+06	2.1426E-14	2.1438E-14	9.5293E-01	1.7436E-03	8.2154E-01
32	8.1873E+06	1.0000E+07	3.2663E-14	3.2682E-14	9.5397E-01	3.2465E-03	8.2479E-01
33	1.0000E+07	1.2214E+07	6.2090E-14	6.2125E-14	9.5639E-01	7.6575E-03	8.3245E-01
34	1.2214E+07	1.3499E+07	2.8612E-14	2.8628E-14	9.5704E-01	2.0481E-03	8.3450E-01
35	1.3499E+07	1.4918E+07	3.6125E-14	3.6145E-14	9.5794E-01	2.8554E-03	8.3735E-01
36	1.4918E+07	1.7500E+07	1.4986E-14	1.4995E-14	9.5862E-01	2.2204E-03	8.3957E-01
37	1.7500E+07	1.9600E+07	9.7600E-15	9.7655E-15	9.5898E-01	1.1761E-03	8.4075E-01
38	1.9600E+07	3.6802E+07	1.8818E-14	1.8829E-14	9.6469E-01	1.9162E-02	8.5991E-01
39	3.6802E+07	6.7719E+07	1.6726E-14	1.6735E-14	9.7380E-01	3.1825E-02	8.9173E-01
40	6.7719E+07	1.2461E+08	1.1532E-14	1.1539E-14	9.8535E-01	4.2490E-02	9.3422E-01
41	1.2461E+08	2.2930E+08	5.7482E-15	5.7515E-15	9.9595E-01	4.5556E-02	9.7978E-01
42	2.2930E+08	4.2193E+08	1.1565E-15	1.1571E-15	9.9988E-01	1.9436E-02	9.9922E-01
43	4.2193E+08	7.7639E+08	2.0095E-17	2.0106E-17	1.0000E+00	7.8397E-04	1.0000E+00
44	7.7639E+08	1.4286E+09	0.0000E+00	0.0000E+00	1.0000E+00	0.0000E+00	1.0000E+00
45	1.4286E+09	2.6288E+09	0.0000E+00	0.0000E+00	1.0000E+00	0.0000E+00	1.0000E+00
46	2.6288E+09	4.8373E+09	0.0000E+00	0.0000E+00	1.0000E+00	0.0000E+00	1.0000E+00

DSTFE5: STGEOM; IRON; BDX, FLUENCE, D = 120CM, DET.2+3; 150MIN

1	2	3	4	5	6	7	8
GRP NO.	LOW BINLIM EV	UPP BINLIM EV	FL-SP INPUT 1/(CM2*EV)	FL-SP NORM. 1/(CM2*EV)	FL-SP NORM. INTEGR.	DE-SP NORM. 1 SV	DE-SP NORM. INTEGR.
1	1.0000E-04	4.1400E-01	0.0000E+00	0.0000E+00	0.0000E+00	0.0000E+00	0.0000E+00
2	4.1400E-01	1.1254E+00	6.4856E-09	6.4826E-09	8.8517E-04	8.5764E-05	8.5764E-05
3	1.1254E+00	2.3824E+00	7.6564E-09	7.6529E-09	2.7316E-03	1.7818E-04	2.6394E-04
4	2.3824E+00	5.0435E+00	1.9606E-09	1.9597E-09	3.7325E-03	9.5820E-05	3.5976E-04
5	5.0435E+00	1.0677E+01	4.9448E-09	4.9425E-09	9.0768E-03	5.0330E-04	8.6307E-04
6	1.0677E+01	2.2603E+01	3.9975E-09	3.9957E-09	1.8223E-02	8.5429E-04	1.7174E-03
7	2.2603E+01	1.0130E+02	1.7234E-09	1.7226E-09	4.4244E-02	2.3698E-03	4.0872E-03
8	1.0130E+02	4.5400E+02	2.6535E-10	2.6523E-10	6.2199E-02	1.5518E-03	5.6390E-03
9	4.5400E+02	1.5846E+03	2.2238E-10	2.2228E-10	1.1043E-01	3.8883E-03	9.5273E-03
10	1.5846E+03	3.3546E+03	1.5285E-10	1.5278E-10	1.6234E-01	3.8342E-03	1.3361E-02
11	3.3546E+03	7.1018E+03	5.9651E-11	5.9624E-11	2.0522E-01	3.0846E-03	1.6446E-02
12	7.1018E+03	1.5034E+04	1.5383E-11	1.5376E-11	2.2863E-01	2.1520E-03	1.8598E-02
13	1.5034E+04	3.1828E+04	2.6887E-11	2.6875E-11	3.1526E-01	1.1147E-02	2.9745E-02
14	3.1828E+04	8.6517E+04	4.5583E-12	4.5562E-12	3.6309E-01	1.2437E-02	4.2182E-02
15	8.6517E+04	1.4996E+05	7.1193E-12	7.1161E-12	4.4974E-01	4.7084E-02	8.9265E-02
16	1.4996E+05	2.2371E+05	9.1009E-12	9.0968E-12	5.7851E-01	9.9461E-02	1.8873E-01
17	2.2371E+05	3.3373E+05	4.3793E-12	4.3773E-12	6.7095E-01	1.0174E-01	2.9047E-01
18	3.3373E+05	4.9787E+05	3.9341E-12	3.9323E-12	7.9483E-01	1.9301E-01	4.8348E-01
19	4.9787E+05	7.4274E+05	1.6243E-12	1.6235E-12	8.7114E-01	1.1888E-01	6.0236E-01
20	7.4274E+05	9.0718E+05	3.1692E-13	3.1678E-13	8.8114E-01	2.1777E-02	6.2414E-01
21	9.0718E+05	1.1080E+06	6.8991E-13	6.8959E-13	9.0772E-01	7.2007E-02	6.9615E-01
22	1.1080E+06	1.3534E+06	2.7845E-13	2.7832E-13	9.2083E-01	3.5514E-02	7.3166E-01
23	1.3534E+06	1.6530E+06	3.0002E-14	2.9988E-14	9.2255E-01	4.6716E-03	7.3633E-01
24	1.6530E+06	2.0190E+06	1.1904E-13	1.1898E-13	9.3091E-01	2.5008E-02	7.6134E-01
25	2.0190E+06	2.4660E+06	1.0303E-13	1.0298E-13	9.3975E-01	2.6435E-02	7.8778E-01
26	2.4660E+06	3.0119E+06	4.5961E-14	4.5940E-14	9.4456E-01	1.5036E-02	8.0281E-01
27	3.0119E+06	3.6788E+06	7.1124E-15	7.1091E-15	9.4547E-01	2.8426E-03	8.0565E-01
28	3.6788E+06	4.4933E+06	7.5616E-15	7.5582E-15	9.4665E-01	3.7276E-03	8.0938E-01
29	4.4933E+06	5.4881E+06	2.7626E-14	2.7614E-14	9.5192E-01	1.6633E-02	8.2602E-01
30	5.4881E+06	6.7032E+06	1.4094E-14	1.4087E-14	9.5521E-01	1.0365E-02	8.3638E-01
31	6.7032E+06	8.1873E+06	0.0000E+00	0.0000E+00	9.5521E-01	0.0000E+00	8.3638E-01
32	8.1873E+06	1.0000E+07	9.7858E-15	9.7813E-15	9.5861E-01	1.0776E-02	8.4716E-01
33	1.0000E+07	1.2214E+07	5.4420E-15	5.4395E-15	9.6092E-01	7.4356E-03	8.5459E-01
34	1.2214E+07	1.3499E+07	1.4179E-14	1.4173E-14	9.6442E-01	1.1244E-02	8.6584E-01
35	1.3499E+07	1.4918E+07	0.0000E+00	0.0000E+00	9.6442E-01	0.0000E+00	8.6584E-01
36	1.4918E+07	1.7500E+07	0.0000E+00	0.0000E+00	9.6442E-01	0.0000E+00	8.6584E-01
37	1.7500E+07	1.9600E+07	2.1639E-15	2.1629E-15	9.6529E-01	2.8888E-03	8.6872E-01
38	1.9600E+07	3.6802E+07	1.2620E-15	1.2614E-15	9.6946E-01	1.4237E-02	8.8296E-01
39	3.6802E+07	6.7719E+07	1.2426E-15	1.2420E-15	9.7683E-01	2.6193E-02	9.0915E-01
40	6.7719E+07	1.2461E+08	1.5181E-15	1.5174E-15	9.9340E-01	6.1969E-02	9.7112E-01
41	1.2461E+08	2.2930E+08	3.2892E-16	3.2877E-16	1.0000E+00	2.8879E-02	1.0000E+00
42	2.2930E+08	4.2193E+08	0.0000E+00	0.0000E+00	1.0000E+00	0.0000E+00	1.0000E+00
43	4.2193E+08	7.7639E+08	0.0000E+00	0.0000E+00	1.0000E+00	0.0000E+00	1.0000E+00
44	7.7639E+08	1.4286E+09	0.0000E+00	0.0000E+00	1.0000E+00	0.0000E+00	1.0000E+00
45	1.4286E+09	2.6288E+09	0.0000E+00	0.0000E+00	1.0000E+00	0.0000E+00	1.0000E+00
46	2.6288E+09	4.8373E+09	0.0000E+00	0.0000E+00	1.0000E+00	0.0000E+00	1.0000E+00